UNIVERSITY OF OKLAHOMA

GRADUATE COLLEGE

APPLICATION OF TIAB's DIRECT SYNTHESIS TECHNIQUE TO TRANSIENT PRESSURE RESPONSE OF NON-NEWTONIAN FLUIDS IN VERTICAL WELLS

A THESIS

SUBMITTED TO THE GRADUATE FACULTY

In partial fulfillment of the requirements for the

Degree of

MASTER OF SCIENCE

By
IRINA DESIREE KATIME MEINDL
Norman, Oklahoma
2000

UNIVERSITY OF OKLAHOMA,
LIBRARIES

Downloaded from SHAREOK. Persistent Handle URL: https://hdl.handle.net/11244/337018

OU
THESIS
MEI
cop. 2

APPLICATION OF TIAB's DIRECT SYNTHESIS TECHNIQUE TO TRANSIENT PRESSURE RESPONSE OF NON-NEWTONIAN FLUIDS IN VERTICAL WELLS

A THESIS APPROVED FOR
THE SCHOOL OF PETROLEUM AND GEOLOGICAL ENGINEERING

BY



©Copyright by IRINA DESIREE KATIME MEINOL 2000
All Rights Reserved

©Copyright by IRINA DESIREE KATIME MEINDL 2000
All Rights Reserved

ACKNOWLEDGMENT

I would like to express my sincere appreciation and gratitude to Dr. Djebbar Tiab for his assistance and encouragement during the completion of this study. I also would like to thank Dr. Samuel Osisanya and Dr. Subhash Shah for their acceptance to be members of my thesis committee.

I am very grateful to PDVSA for the financial support granted in the form of a scholarship, which has made my graduate studies possible.

I wish to thank all faculty, staff and students for their attitude and support. Especially to Mr. Freddy Escobar and Ms. Margiori Rivas, for all the help they gave me to finish this work. To my Industrial Advisor, Mr. Cesar Rodriguez and all the people that works in the Extra-heavy oil Department, PDVSA, in San Tome, Venezuela, for always being there when I needed any information and support.

Finally, I dedicate this study to my parents for their encouragement and support during these two years.

TABLE OF CONTENTS

ACKNOWLEDGMENTS iv

TABLE OF CONTENTS v

LIST OF TABLES vii

LIST OF FIGURE viii

ABSTRACT xi

CHAPTER

I INTRODUCTION 1

1.1. Pressure transient tests 1

1.2 Non-Newtonian fluid flow 5

1.3 Non-Newtonian Fluid Pressure transient analysis 13

1.4 Interpretation methods 16

1.5. Objectives 20

II PRESSURE RESPONSE OF NON-NEWTONIAN FLUID IN AN INFINITE RESERVOIR 21

2.1 Mathematical Model 21

2.1.1 Well located in an infinite reservoir 21

2.1.2 Characteristic points and Straight lines 24

2.1.3 Procedures 48

2.1.4 Application 57

III PRESSURE RESPONSE OF NON-NEWTONIAN FLUID IN THE PRESENCE OF A LINEAR BOUNDARY 64

3.1 Well located near a single linear boundary 65

IV SUMMARY, CONCLUSIONS AND RECOMMENDATIONS 75

NOMENCLATURE 78

REFERENCES 81

APPENDIX A 86

LIST OF TABLES

TABLE		Page
2.1	Pressure and pressure derivative data for a falloff test	58
2.2	Comparison of results	63

LIST OF FIGURES

FIGURE		Page
1.1	Examples of Time-independent non-Newtonian Fluids	8
1.2	Hysteresis loop found by shearing a thixotropic fluid at a Constantly increasing and decreasing rate	9
1.3	Behavior of a thixotropic fluid allowed to rest for differing Times from a state of just having been sheared	10
1.4	A new set of type curve for a well with wellbore storage and skin	19
2.1	Pressure and Pressure derivative curves for Newtonian fluid	25
2.2	Pressure and Pressure derivative curves for flow behavior Index, n = 0.8	26
2.3	Pressure and Pressure derivative curves for flow behavior Index, n = 0.6	27
2.4	Pressure and Pressure derivative curves for flow behavior Index, n = 0.4	28
2.5	Pressure and Pressure derivative curves for flow behavior Index, n = 0.2	29
2.6	Pressure derivative curves for different flow behavior index	31

2.7 Starting time of the infinite-acting radial flow line for Different n values 34

2.8 Relationship of intersection points with the unit-slope line And different n – values 36

2.9 Correlation of the maximum point coordinates for n=1 38

2.10 Correlation of the maximum point coordinates for n=0.8 38

2.11 Correlation of the maximum point coordinates for n=0.6 39

2.12 Correlation of the maximum point coordinates for n=0.4 39

2.13 Correlation of the maximum point coordinates for n=0.2 40

2.14 General relationship of the maximum points and the different flow behavior indexes 40

2.15 Relationship of $\log(C_De^{2S})$ and the coordinates of the maximum points for n = 1 42

2.16 Relationship of $\log(C_De^{2S})$ and the coordinates of the maximum points for n = 0.8 42

2.17 Relationship of $\log(C_De^{2S})$ and the coordinates of the maximum points for n = 0.6 43

2.18 Relationship of $\log(C_De^{2S})$ and the coordinates of the maximum points for n = 0.4 43

2.19 Relationship of $\log(C_De^{2S})$ and the coordinates of the maximum points for n = 0.2 44

2.20 Values of the intersection points for different n values in the eqs. 2.41 and 2.42 44

2.21 Relationship between the slope of the infinite-acting radial flow line and the flow behavior index, n 49

2.22 Example of Falloff test 59

3.1 A well near a single linear boundary (method of the images) 64

3.2 Pressure derivative curves for a well near a no-flow boundary 68

3.3 Pressure derivative curves for a well near a constant-pressure Boundary 70

3.4 Relationship between the intersection of the radial flow line and a constant-pressure boundar and n 74

3.5 Relationship between the end of the infinite-radial flow Regime and n in the presence of a linear boundary 74

ABSTRACT

Non-Newtonian fluids are very common during drilling, fracture operations and enhanced oil recovery processes. When a reservoir contains a non-Newtonian fluid such as those injected during polymer flood or the production of heavy oil, well test data cannot be interpreted using Newtonian fluid flow models. The resulting analysis would be erroneous because non-Newtonian fluids behave rather differently.

These results suggest the need for a thorough study of the behavior of non-Newtonian fluids in the reservoir and also a new look at the flow of those fluids in porous media.

This study presents an interpretation technique for pressure behavior of non-Newtonian fluid flow in a homogeneous reservoir without type-curve Matching. The inclusion of a no-flow and/or a constant pressure line is also investigated.

First, the TSD (Tiab's Direct Synthesis) technique was applied for analyzing the pressure behavior of a well located in (1) an infinite reservoir and, (2) near a linear boundary where wellbore storage and skin effects were considered. The analysis required the generation of type-curve sets for different wellbore storage and skin values.

A step-by-step procedure is presented for the calculation of the reservoir parameters: the permeability/viscosity ratio, wellbore storage coefficient, skin factor and the distance to the nearest boundary without the use of type-curve Matching. The procedure is illustrated by a numerical example.

CHAPTER I

INTRODUCTION

1.1) Pressure transient tests:

Pressure transient techniques, such as pressure buildup, drawdown, injectivity, falloff, and interference tests, are an important part of reservoir and production engineering. Pressure transient testing includes generating and measuring pressure variations and time in wells and the estimation of rock, fluid and well properties. The information obtained from transient testing includes wellbore volume, damage, and improvement in reservoir pressure; permeability; porosity; reserves; reservoir and fluid discontinuities; and other related data. All this information can be used to help analyze, improve, and forecast reservoir performance.

There are several tests used to monitor changes of well conditions. During the life of a reservoir, it is very useful to monitor any change in pressure response in order to identify the candidates for workover or/and stimulation, and track the movement of fluid fronts within the reservoir, such as those may be seen in water flooding or in-situ combustion. Also they can be used to estimate whether the reservoir boundaries are closed or open (with aquifer support or a free surface).

The type of test to be performed is governed by the reservoir characteristics to be examined.

a) Drawdown Test:

In this type of test, a well that is static, stable and shut-in is opened to flow at a constant rate. Drawdown testing is a good method of reservoir limit testing, since the time required to observe a boundary response is long and operating fluctuations in flow rate become less significant over long periods. It is used to define the shape and geometry of the reservoir.

b) Buildup Test:

In a buildup test, a well that is already flowing is shut-in and the downhole pressure is measured as the pressure builds up. This test can be used to characterize the inner boundaries and to know the average reservoir pressure. This type of test has two major disadvantages.

1) It may be difficult to achieve a constant production rate prior to the shut-in.

2) Production is lost while the well is shut-in.

c) Injection and Falloff Tests:

An injection test is identical to a drawdown test, except that flow is into the well rather than out of it.

A falloff test measures the pressure decline subsequent to the closure of an injection. It is conceptually identical to a buildup test.

Injection and falloff test interpretation is more difficult due to the multiphase effect if the injected fluid is not the same as the original reservoir fluid.

d) Interference Test:

In this test, one well is produced and pressure is observed in a different well. The test monitors pressure changes in the reservoir, at a distance from the original producing well. They are useful to characterize reservoir properties over a greater length scale than single-well tests. They are used (1) to determine whether two or more wells are in pressure communication and (2) when communication exists, to provide estimates of permeability and porosity/compressibility product in the vicinity of the tested wells.

e) Drill Stem Test (DST):

This test is normally run in a zone of undetermined potential in a well being drilled, although they are sometimes run in known productive zones in development wells. Analysis of the DST transient pressure data can provide an estimate of formation properties and wellbore damage. Most DST's include a short production period; a short shut-in period, a longer flow period and a longer shut–in period.

Over the last four decades, a great deal of information concerning well test analysis has appeared in the literature. In addition, the well testing analysis techniques have progressed rapidly since the introduction of the pressure derivative approach.

As early as 1937, Muskat[1] suggested the first pressure buildup analysis approach to the petroleum industry. He related the slope of the straight-line portion on the semilog plot of pressure versus time with the flow capacity of the reservoir.

In 1950, Miller, Dyes and Hutchinson[2] also established a method for pressure buildup analysis. They suggested that the pressure versus the log of Δt be plotted. Their work included the estimation of flow capacity and static reservoir pressure.

In 1951, Horner[3] proposed a new technique in which the buildup pressure is plotted versus the log of $\left(\frac{t+\Delta t}{\Delta t}\right)$ for a well located in an infinite reservoir. This technique is very useful to estimate flow capacity, static reservoir pressure and the distance to the nearest boundary.

The short-time well test shown by Ramey[4] can be used to supplement conventional interpretation of the straight-line portion of pressure buildup analysis. This study was done by using type-curve matching.

Tiab[5], and Tiab and Kumar[6] studied the behavior of time rate of change of dimensionless pressure for a line source well and its application to interference analysis. They also improved the calculation of the distance of the well to the nearest boundary.

Most of the material reviewed so far is related to homogeneous and isotropic reservoirs, but they can be extended for the inclusion of heterogeneities. The presence of heterogeneities in a reservoir, such as faults or change in rock and fluid properties, significantly affects the wellbore pressure behavior. Therefore, an accurate reservoir description from pressure transient-analysis is critical for optimizing the hydrocarbon recovery.

1.2) Non-Newtonian Fluid Flow:

Since the pressure behavior of non-Newtonian fluids is the main objective of this work, it is appropriate to review some of the literature on the transient flow analysis of this type of fluid.

There is a vast amount of information in the literature on elastic properties of polymer solutions, viscoelasticity, and viscoelastic flow of non-Newtonian fluids in porous media. However, most of the areas of study still lack complete explanation.

Although many fluids in nature are Newtonian, there are many fluids of practical importance that do not even approximate a linear relationship. They are known as non-Newtonian Fluids.

Use of non-Newtonian fluids in the petroleum industry is not new. Fluids of this type have been used for many years as fracturing agents and drilling muds. There are three general classifications of non-Newtonian fluids:

1. **Time-Independent Non-Newtonian Fluids**, in which the shear-strain rate is single-valued but nonlinear of shear stress. The strain rate of these fluids is as follows:

$$\sigma_{ij} = f(e_{ij}) \qquad \text{.....(1.1)}$$

Examples of this type of fluids are the Bingham plastic, pseudoplastic and dilatant fluids.

The Bingham plastic concept is a close approximation to many real fluids, including some slurries, greases, paint and some suspensions of finely divided particles such as clay in water. This type of fluid behaves like a solid until the yield stress, τ_y, is exceeded; then it behaves like a viscous Newtonian fluid with viscosity μ_p. The shear stress may be expressed as:

$$\tau = \tau_y + \mu_p \gamma \qquad \tau > \tau_y$$

$$\gamma = 0 \qquad \tau < \tau_y \qquad (1.2)$$

Pseudoplastic and dilatant fluids do not have a yield stress. The pseudoplastic fluid has a progressively decreasing slope of shear stress versus shear strain rate, which tends to become constant for very large values of shear stress. Many models have been developed to describe pseudoplastic flow, but the simplest and perhaps most useful is the Ostwald de Waele power-law relationship

$$\tau = k\gamma^n \qquad (n < 1) \qquad \text{.....(1.3)}$$

where k and n are constants for a particular fluid. The parameter k is a measure of the consistency of the fluid and n is a measure of how much the fluid deviates from a Newtonian fluid for which $k = \mu$ and $n = 1$.

Several more complex models of pseudoplastic fluids have been proposed, but they lead to rather complex representations and will not be discussed here.

Dilatant fluids are similar to pseudoplastic fluids except that the apparent viscosity increases with strain rate. The Power-law model may also be used here, except that the exponent n is now greater than unity. Figure 1.1 shows the stress-strain rate relationship for these fluids.

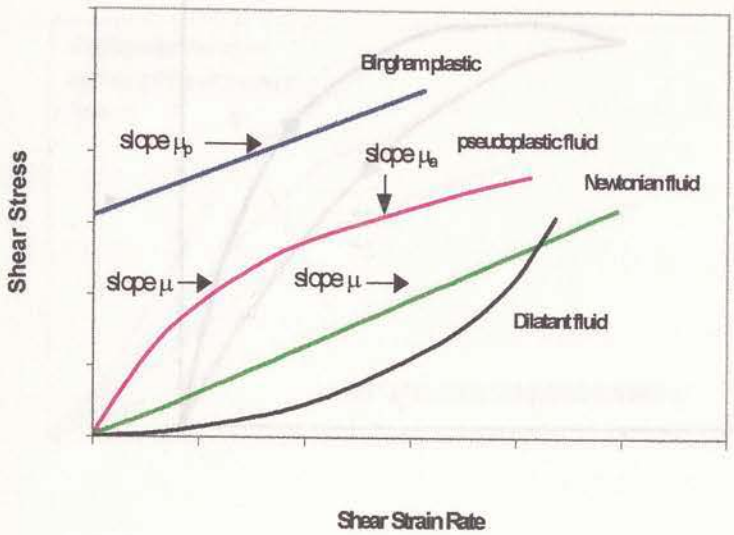

Figure 1.1 – Examples of time-independent non-Newtonian fluids

2. **Time-dependent Non-Newtonian Fluids**, in which the shearing rate is not a single-valued function of the shear stress and may depend on the previous shear stress history of the fluid. The shear strain rate versus shear stress curve may form a hysteresis loop. Figure 1.2 illustrates the hysteresis loop found by shearing a thixotropic fluid at a constantly increasing rate and then at a constantly decreasing rate.

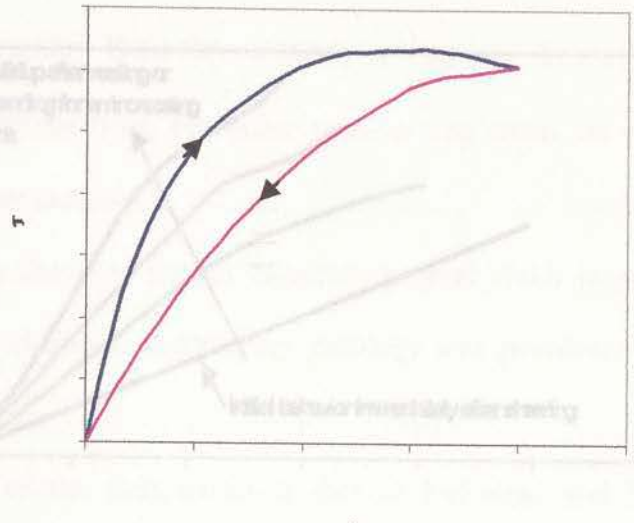

Figure 1.2 – Hysteresis loop found by shearing a thixotropic fluid at a constantly increasing and decreasing rate

Time-dependent fluids have an apparent viscosity that depends not only on the shear rate, as just described above, but also on the time for which the shear has been applied. There are two general classes of time-dependent fluids, thixotropic fluids and rheopectic fluids. The shear stress decreases with time in a thixotropic fluid and increases with time in a rheopectic fluid at a constant shear rate. The behavior of a thixotropic fluid is illustrated by Fig. 1.3. The apparent viscosity depends on both the shear rate and the length of time of shearing.

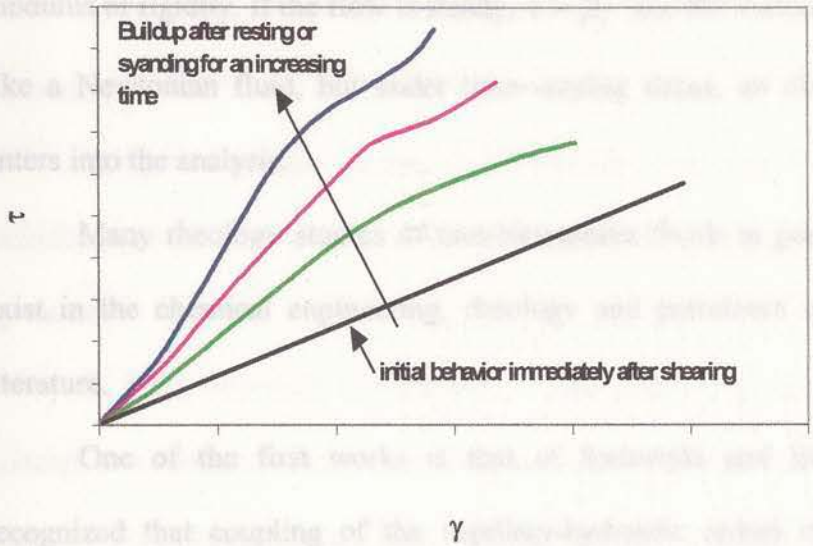

Figure 1.3 – Behavior of a thixotropic fluid allowed resting for differing times from a state of just having been sheared

3. **Viscoelastic Fluids**, in which shear strain as well as shear strain rate are related to the shear stress. Because of the partially elastic property of these fluids, not all the energy of shear deformation is dissipated, but some may be stored in the fluid as elastic strain energy. They can be rather complex and exhibit both viscous and elastic-type behavior. The simplest model of viscoelastic materials is the Maxwell liquid model, which assumes that the fluid is Newtonian in viscosity and obeys Hooke's law for the elastic behavior. The stress-strain rate relationship is

$$\tau + \left(\frac{\mu}{\lambda}\right)\dot{\tau} = \mu\gamma \quad \text{.....(1.4)}$$

where $\dot{\tau}$ is the time derivative of stress state, μ is the viscosity and λ is the modulus of rigidity. If the flow is steady, $\tau = \mu\gamma$ and the material behaves like a Newtonian fluid, but under time-varying stress, an elastic effect enters into the analysis.

Many rheology studies of non-Newtonian fluids in porous media exist in the chemical engineering, rheology and petroleum engineering literature.

One of the first works is that of Sadowski and Bird[8,9], who recognized that coupling of the capillary-hydraulic radius model of a porous medium with a viscosity function ignores time-dependent elastic phenomena. They also reasoned that no elastic effects would be observed provided the fluid relaxation time is small compared to transit time through a contraction or expansion in a tortuous channel of the porous medium. Conversely, they expected major elastic effects as the fluid relaxation time becomes large compared to the transit time. In their experimental work, Sadowski and Bird[8,9] observed significant deviations from the modified Darcy's law and found that introduction of a correction factor in the Ellis model for non-Newtonian flow eliminated these deviations.

However, Astarita[10] argued that the relaxation time defined by Sadowski and Bird[8,9] is related only to $\mu_{NN}(\dot{\gamma}_{xy})$ and not to the viscoelastic properties.

Savins[11] has also shown that Sadowski and Bird[8,9] results fit pseudoplastic fluid behavior exactly, if analyzed using a generalized scale-up model.

In 1967, Marshall and Metzner[12] used Reiner's Deborah number concept in a similar fashion to the Ellis number of Sadowski and Bird[8,9] to identify viscoelastic effects. They modeled porous media by considering flow in the frusta of right cylindrical cones, where converging and diverging sections would represent flow into and out of constrictions in the media. They showed experimentally that the Deborah number could be an appropriate parameter to detect viscoelastic effects in porous media.

Using Maxwell model as the constitutive equation, Wissler[13] performed a third order perturbation analysis of flow of a viscoelastic fluid through a conical-contraction-expansion model. Coupling the constitutive model with the continuity and momentum equations in cylindrical coordinates and assuming incompressible fluid, he derived an equation that expresses the viscoelastic pressure drop over a conical contraction in porous media. Schummer[14] did a similar perturbation analysis for both a conical section and a convergent channel.

In a study on turbulent flow properties of viscoelastic fluids, Seyer and Metzner[15] reported that the abnormally high resistance of viscoelastic fluids to sudden deformations and to stretching effects turbulent velocity fields appreciably. They provided new correlations for friction factors of viscoelastic fluids under turbulent flow conditions.

During the seventies, research on viscoelastic flow through porous media was relatively abundant but limited to petroleum engineering literature.

1.3) Non-Newtonian fluid pressure transient analysis

The subject of transient flow of power-law fluids in porous media is very new to well testing. Van Poollen and Jargon[16] wrote the first paper in 1969. They investigated both steady and unsteady-state flow of non-Newtonian fluids using a numerical simulator that accounts for variable viscosity. They showed that the drawdown curves for power-law fluids do not exhibit the straight-line relationship as they exist for Newtonian fluids, and the slope of P_D versus the log of t_D could be used to calculate the average viscosity in the non-Newtonian slug region.

Odeh and Yang[17] proposed analysis methods based on the solution of the diffusivity equation in which viscosity was a shear rate dependent variable. They recommended that ΔP be plotted versus t to obtain the

permeability of a formation from injectivity that contains a power-law fluid.

Ikoku and Ramey[18] derived a new partial differential equation for radial flow of power-law fluid through porous media, using the modified Blake-Kozeny model and the Ostwald de Waele power-law relationship. They obtained two slightly different long-time approximate solutions for the case of constant-rate injection into an infinitely large reservoir. These solutions made the calculation of effective mobility possible from the slope of the straight line obtained when ΔP is plotted versus $t^{\frac{1-n}{3-n}}$. An in-situ value of n could be found from the late-time straight line obtained on a log-log plot of ΔP versus t or from the p-intercept at t = 0 on the P versus $t^{\frac{1-n}{3-n}}$ plot. Ikoku and Ramey[18] also developed relationships to calculate skin and radius of investigation.

In a later investigation, Ikoku and Ramey[19] solved the rigorous, nonlinear partial differential equation using the Douglas-Jones predictor-corrector method, and showed that errors introduced by the approximate, linear equation were small and decreased with increasing value of the flow behavior index, n.

Ikoku and Ramey[20] also investigated flow of power-law fluids in finite circular reservoirs, and skin and wellbore storage effects on early

time transient response. They presented type curves to be used under these conditions.

Lund and Ikoku[21] extended Ikoku and Ramey's methods to transient flow in power-law and Newtonian fluid composite reservoirs.

In 1985, Huh and Snow[22], using an adaptation of the Carreau model, solved the pressure transient equation simultaneously with the polymer transport equation to obtain the pressure response for any assumed radial distribution of polymer within the reservoir. Thus, for a given distribution of polymer in the reservoir, appropriate formation parameters such as porosity, permeability and thickness can be deduced. Unlike previous solutions for non-Newtonian rheology, the nonlinear character of the equation was preserved.

Vongvuthipornchai and Raghavan[23] examined pressure falloff behavior dominated by wellbore storage and skin subsequent to the injection of a non-Newtonian power-law fluid. They also demonstrated that for certain combinations of skin factor and power-law index, n, the effective wellbore radius vanishes. To improve analysis procedures, they examined the use of the pressure derivative technique and discussed the advantages of this method in analyzing pressure falloff data.

In 1992, Olarewaju[24] demonstrated the difference in behavior between a Newtonian and a non-Newtonian fluid in homogeneous and

double-porosity reservoirs and presented practical pressure and derivative type curve solutions for analyzing data from those reservoirs.

1.4) Interpretation methods:

Well tests have been used for many years for evaluating reservoir characteristics, and numerous methods of interpretation have been proposed in the past. A number of these methods has become very popular, and are usually referred to as "conventional." In the last twenty years, many others have been developed, which are often called "modern." Those interpretation methods published by Horner and Miller, Dyes, and Hutchinson constitute the so-called "conventional" techniques. These methods can be used only for tests of sufficient duration, if and when radial flow is established in the reservoir and boundary effects are not significant.

Due to the improvements in measuring devices and the availability of more sophisticated reservoir models, well tests can now provide more information on reservoirs than in the past. Basically, the earlier the test data, the more detailed the reservoir information; or in other words, different ranges of test data yield reservoir parameters characterizing the reservoir behavior on different scales. This type of detailed information is

the usual target of "modern" analysis. The modern techniques include Type-curve matching and the Direct synthesis methods.

a) **Type-curve Matching:**

This technique is not new. Theis first introduced it in 1935 for interpreting interference tests in aquifers. During the seventies, Ramey[4] and Argawal[25] introduced it in the literature. Then, other investigators[26-30] improved the technique to extend it for analyzing different reservoir models and flow regimes. The method can be used to analyze data from drawdown, buildup, interference and constant-pressure testing.

The type-curves are generated in dimensionless parameters that result from the real parameters multiplied by a term, which include some characteristics of the system.

The log-log type-curve plots of these dimensionless parameters (P_D, t_D) and its derivatives provide more information about the system than the semilog plot of the pressure versus time. This is due to the sensitivity of the derivative response to any change in the reservoir behavior at any time of the test.

The matching technique is a process that fits the real data points to the dimensionless points on the type-curve. The procedure consists of overlying the real data plot on a same-size type-curve, moving the former

UNIVERSITY OF OKLAHOMA
LIBRARIES

until the best match is obtained with one curve-set on the type-curve plot. Then, the real and dimensionless coordinates of the points on the graph are used to determine the parameters of the real system.

b) Tiab's Direct Synthesis (TDS):

TDS technique is a procedure that uses the unique characteristics of the log-log plot of pressure and pressure derivative versus time to determine reservoir and fluid properties without type-curve matching.[31] The technique is a step-by-step procedure which is used to calculate reservoir and fluid properties by using appropriate equations for the points, slopes and times shown by the log-log plot of pressure and pressure derivative versus time for a well in an infinite reservoir. (Figure 1.4)[30]

The following characteristics of the pressure and pressure derivatives curves for a well in an infinite reservoir system may be considered.

(1) Unit slopes during early time for both pressure and pressure derivatives, which corresponds to pure wellbore storage flow.

(2) Maximum points of the derivative curves on the wellbore storage dominated flow region with the coordinates $\left[\left(\frac{t_D}{C_D}\right)P_D'\right]_x$ and $\left[\left(\frac{t_D}{C_D}\right)\right]_x$.

(3) A horizontal straight line at $\left[\left(\frac{t_D}{C_D}\right)P_D'\right]_r = 0.5$ at late time (for Newtonian fluids), following the pure wellbore storage flow regime region, corresponding to the infinite radial flow regime. In the case of non-Newtonian fluids, in which the flow behavior index, n, takes values between 0 and 1, $\left[\left(\frac{t_D}{C_D}\right)P_D'\right]_r = f(n)$.

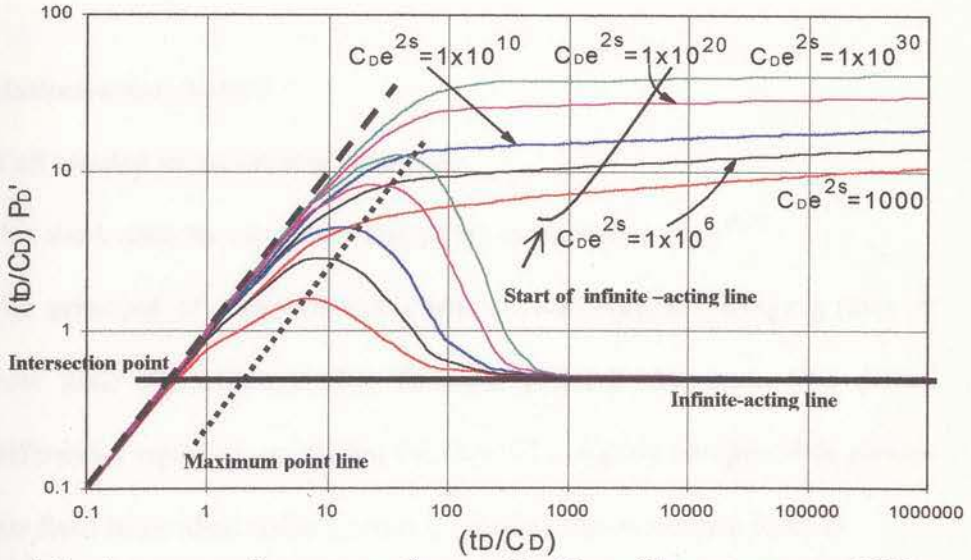

Figure 1.4 - A new set of type curve for a well with wellbore storage and Skin

1.5) Objectives

This study analyzes the pressure behavior of non-Newtonian fluid flow in a homogeneous reservoir. It also analyzes the pressure behavior of the pressure data in the presence of a single linear boundary.

First, the TDS technique is applied for analyzing the pressure behavior of a well located in (1) an infinite reservoir and, (2) near a linear boundary. The wellbore storage and skin effects are considered. The analysis requires the generation of type-curve sets for different wellbore storage and skin coefficients.

A step-by-step procedure is presented for the calculation of the reservoir parameters: mobility ratio, wellbore storage coefficient, skin factor and distance to the nearest boundary.

CHAPTER II

PRESSURE RESPONSE OF NON-NEWTONIAN FLUID IN AN INFINITE RESERVOIR

The transient pressure behavior in wells producing or/and injecting non-Newtonian fluids is of considerable interest because of the large number of enhanced oil recovery projects now in operation. As a result of a number of studies over the past two decades an increased understanding of non-Newtonian fluid behavior in petroleum reservoirs has been obtained. It is generally believed that many of the non-Newtonian fluids used in enhanced oil recovery processes are pseudoplastic in nature and a power-law model can approximate their rheology.

2.1) Mathematical Model

2.1.1) Well located in an infinite reservoir

This work uses the model developed by Ikoku and Ramey[18,20].

The principle of superposition enables us to analyze changing rates of flow from the solution of a constant terminal rate case. The partial differential equation describing the flow of a slightly compressible power-law fluid in an ideal radial system is given in dimensionless form as

$$\frac{\partial^2 P_D}{\partial r_D^2}+\frac{n}{r_D}\frac{\partial P_D}{\partial r_D}=r_D^{1-n}\frac{\partial P_D}{\partial t_D} \quad \text{.....(2.1)}$$

where

$$P_D=\frac{p-p_i}{\left(\frac{q}{2\pi h}\right)^n\frac{\mu_{eff}r_w^{1-n}}{k}} \quad \text{.....(2.2)}$$

$$r_D=\frac{r}{r_w} \quad \text{.....(2.3)}$$

$$t_D=\frac{t}{Gr_w^{3-n}} \quad \text{.....(2.4)}$$

$$G=\frac{n\phi c_t\mu_{eff}}{k}\left(\frac{2\pi h}{q}\right)^{1-n} \quad \text{.....(2.5)}$$

$$C_D=\frac{C}{2\pi hn\phi c_t r_w^2} \quad \text{.....(2.6)}$$

The initial and boundary conditions for this problem are

(1) $P_D(r_D,0)=0$ .....(2.7)

(2) $P_D(r_D,t_D)\to 0$ as $r_D\to\infty$ .....(2.8)

(3) $C_D\frac{dP_{Dw}}{dt_D}-\frac{\partial P_D}{\partial r_D}(1,t_D)=1$

$$P_{Dw}-P_D(1,t_D)-S\frac{\partial P_D}{\partial r_D}(1,t_D)=0 \quad \text{.....(2.9)}$$

The constant terminal rate solution for an infinitely large reservoir in the Laplace space including skin factor and wellbore storage for a single-porosity non-Newtonian flow, is:

$$\overline{P}_{Dw}(z)=\frac{K_v\left(\beta\sqrt{z}r_D^{1/\beta}\right)+S\sqrt{z}K_\beta\left(\beta\sqrt{s}\right)}{z\left(\sqrt{z}K_\beta\left(\beta\sqrt{z}\right)+zC_D\left[K_v\left(\beta\sqrt{z}\right)+S\sqrt{z}K_\beta\left(\beta\sqrt{z}\right)\right]\right)} \quad \text{.....(2.10)}$$

where $\beta=\dfrac{2}{3-n}$ and $v=\dfrac{1-n}{3-n}$.

Here $\overline{P}_{Dw}(z)$ denotes the Laplace transform of $P_D(t_D)$ at the wellbore, z is the Laplace variable and $K_v(x)$ is the modified Bessel function of the order v.

To obtain the real space solution for the reservoir pressure behavior as a function of time in dimensionless form, one has to accomplish it with the numerical inversion scheme presented by Stehfest[32].

The solution for a Newtonian fluid with skin factor and wellbore storage is given by:

$$\overline{P}_{wD}=\frac{K_0\left(\sqrt{s}\right)+S\sqrt{s}K_1\left(\sqrt{s}\right)}{s\left(\sqrt{s}K_1\left(\sqrt{s}\right)+sC_D\left[K_0\left(\sqrt{s}\right)+S\sqrt{s}K_1\left(\sqrt{s}\right)\right]\right)} \quad \text{.....(2.11)}$$

The scheme is based upon the following equation:

$$P_D(t_D)=\frac{\ln 2}{t_D}\sum_{i=1}^{N}V_i\overline{P}_D(s_i) \quad \text{.....(2.12)}$$

Where $$s_i = \frac{\ln 2}{t_D} i \quad \text{.....(2.13)}$$

And

$$V_i = (-1)^{\frac{N}{2}+i} \sum_{x=\left(\frac{i+1}{2}\right)}^{\max\left(\frac{N}{2},i\right)} \frac{x^{\frac{N}{2}}(2x)!}{\left(\frac{N}{2}-x\right)!\,x!\,(x-1)!\,(i-x)!\,(2x-i)!} \quad \text{.....(2.14)}$$

V_i depends only on N and its properties are such that for a given value of N, the V_i's sum to zero and $|V_i|$ tends to increase as N increases. The V_i's need to be calculated only once for a chosen value of N. The value of N must be chosen by numerical experiments and its value may change with time. Usually the accuracy of the $F_a(t)$ increases as N increases. The N is usually in the range of $8<N<12$.

In this study, the Tiab's Direct Synthesis[31] is applied in order to avoid the generation of different sets of type-curve for each flow behavior index, n. This approach is very useful when the early-time unit slope line and/or the late-time infinite-acting radial flow line are not well developed due to the lack of data.

2.1.2) Characteristic points and straight lines

The log-log plot of dimensionless pressure and pressure derivatives versus time, Figures 2.1 through 2.5, have several unique characteristics:

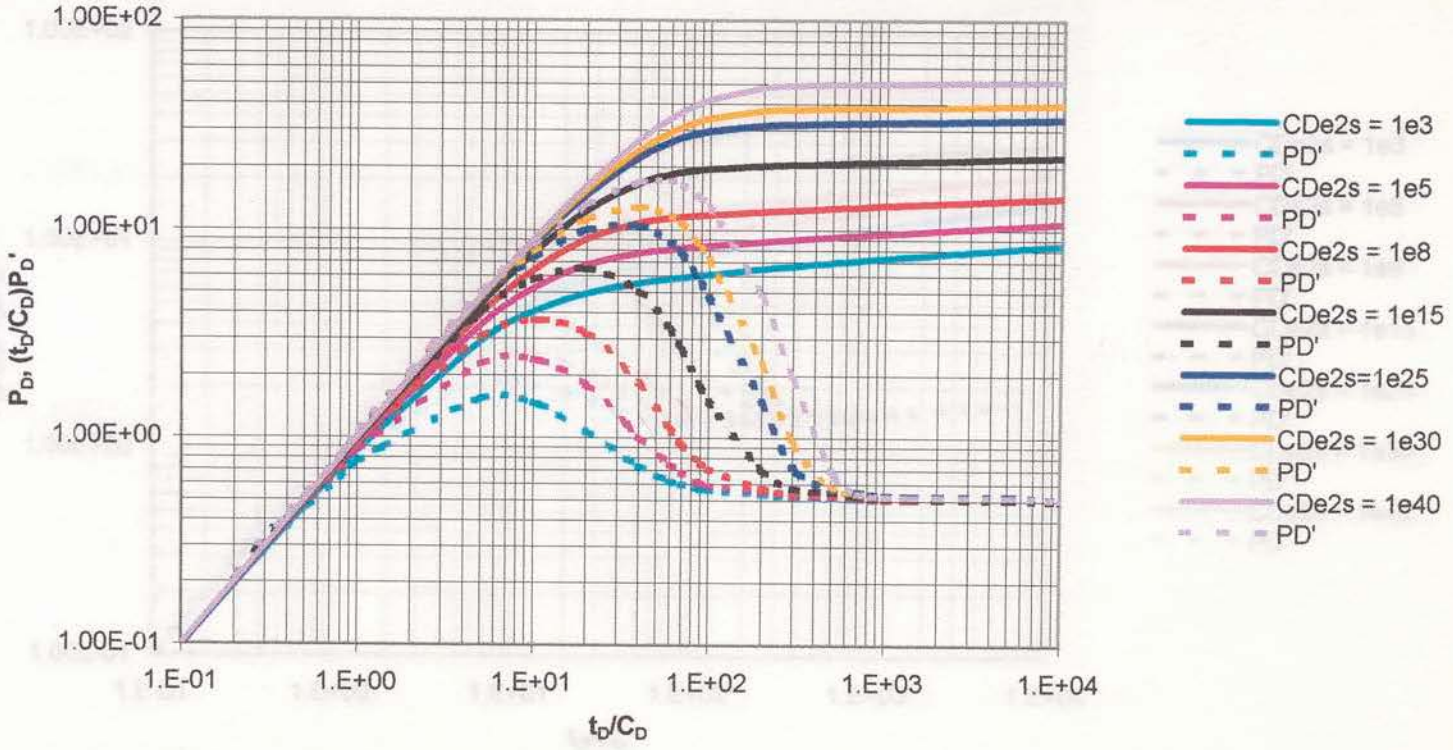

Figure 2.1 - Pressure and Pressure derivative curves for newtonian fluid, n = 1.0

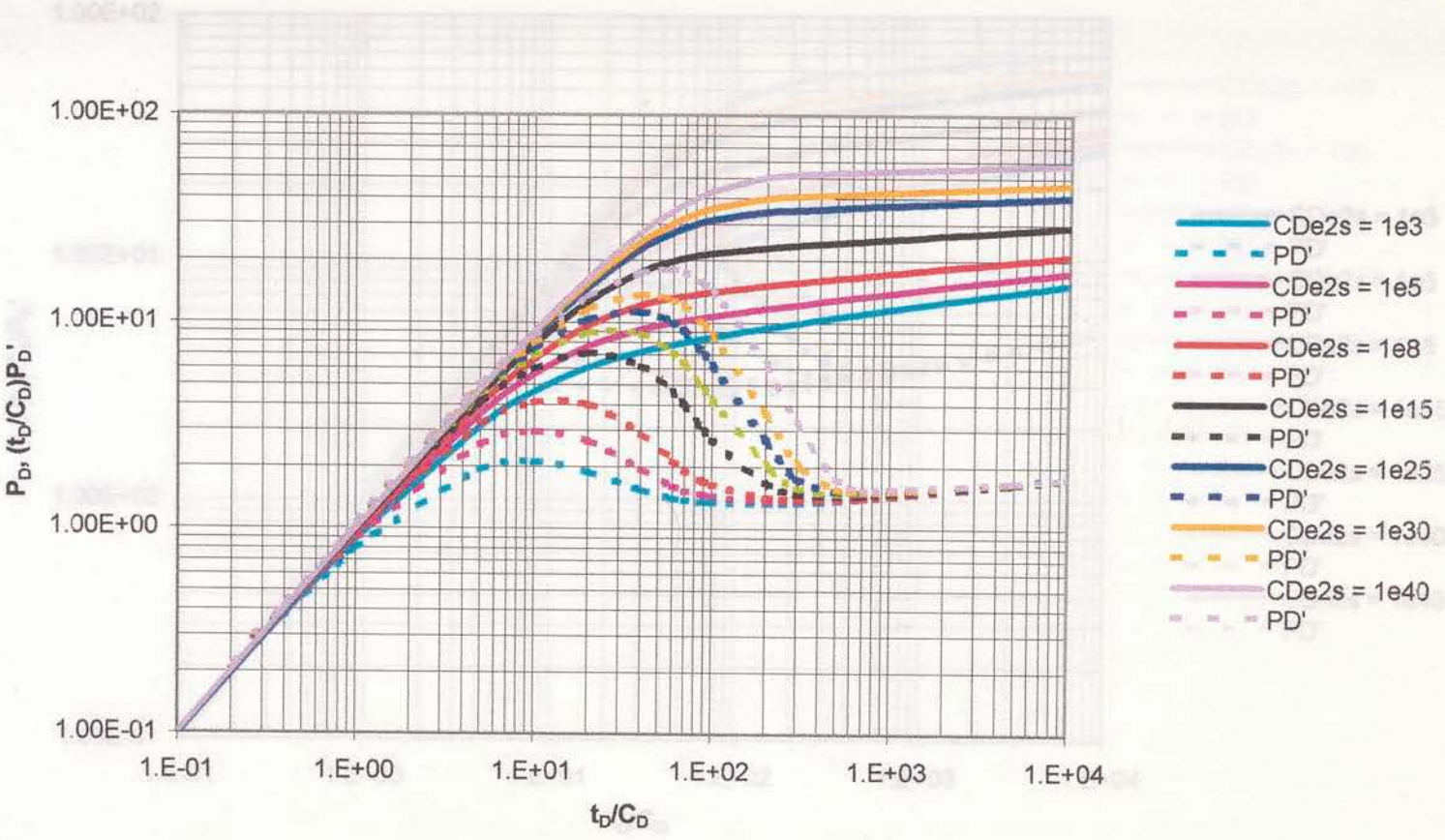

Figure 2.2 - Pressure and Pressure derivative curves for flow behavior index, n =0.8

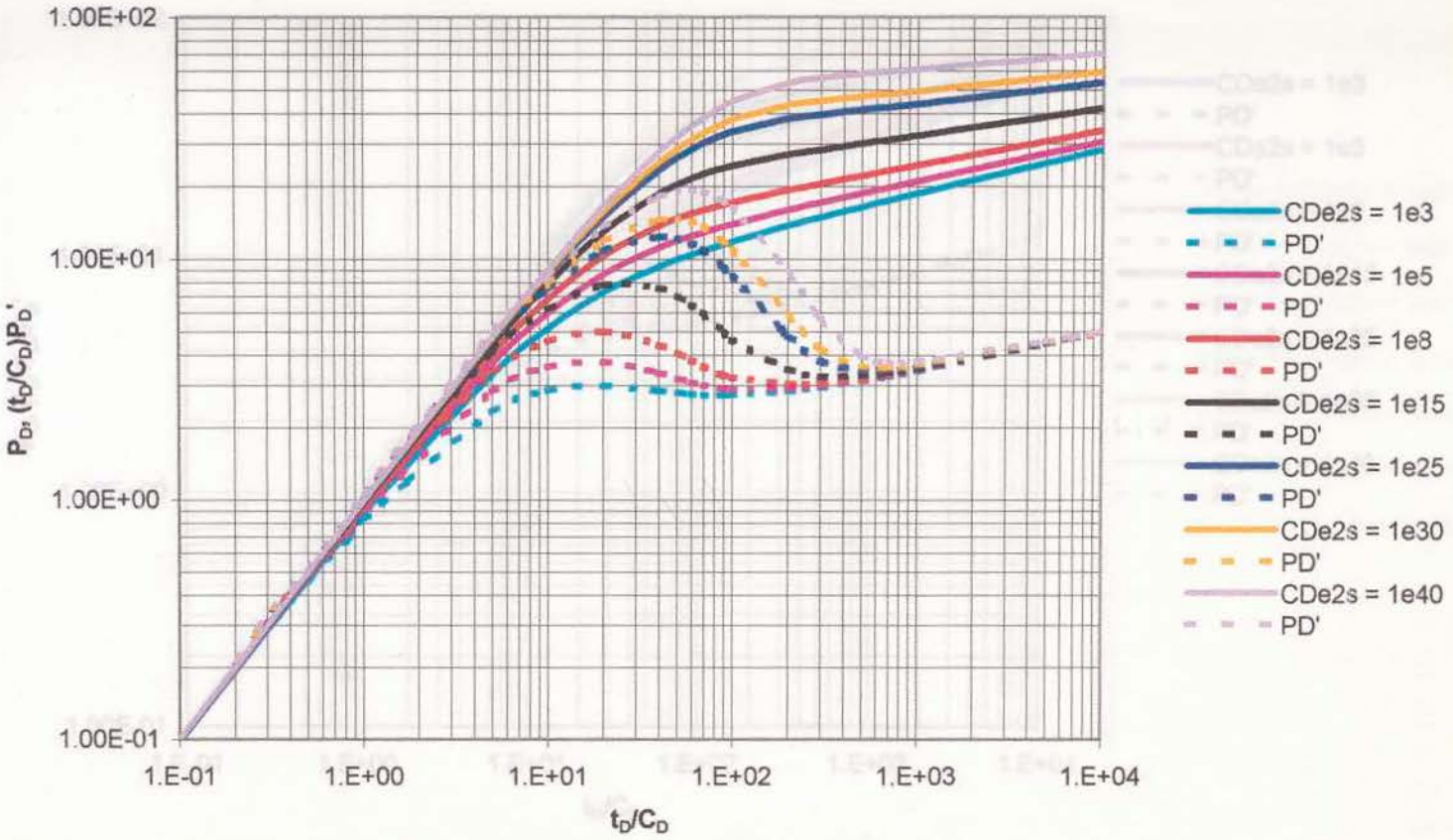

Figure 2.3 - Pressure and Pressure derivative curves for flow behavior index, n = 0.6

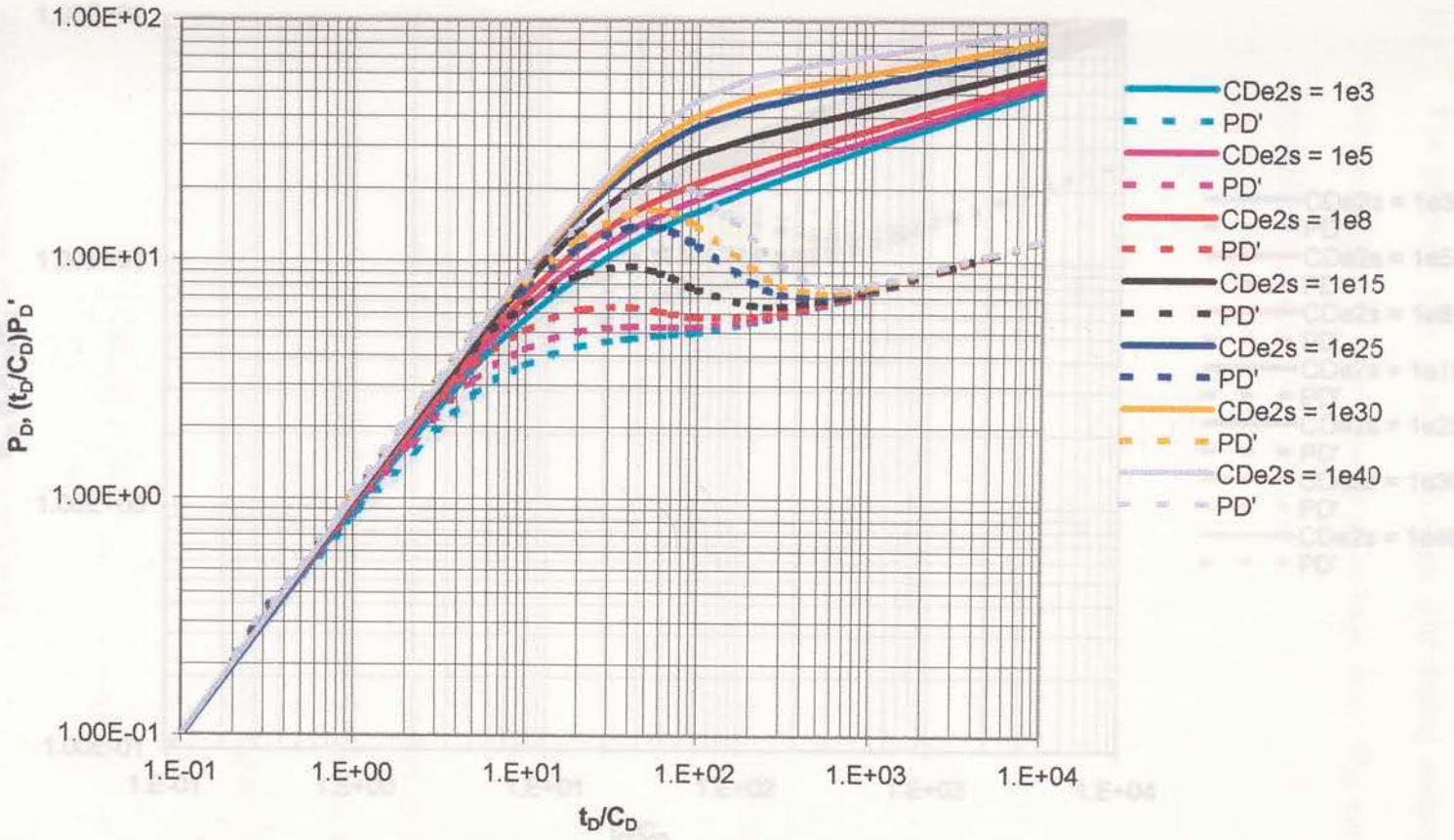

Figure 2.4 - Pressure and Pressure derivative curves for flow behavior index, n = 0.4

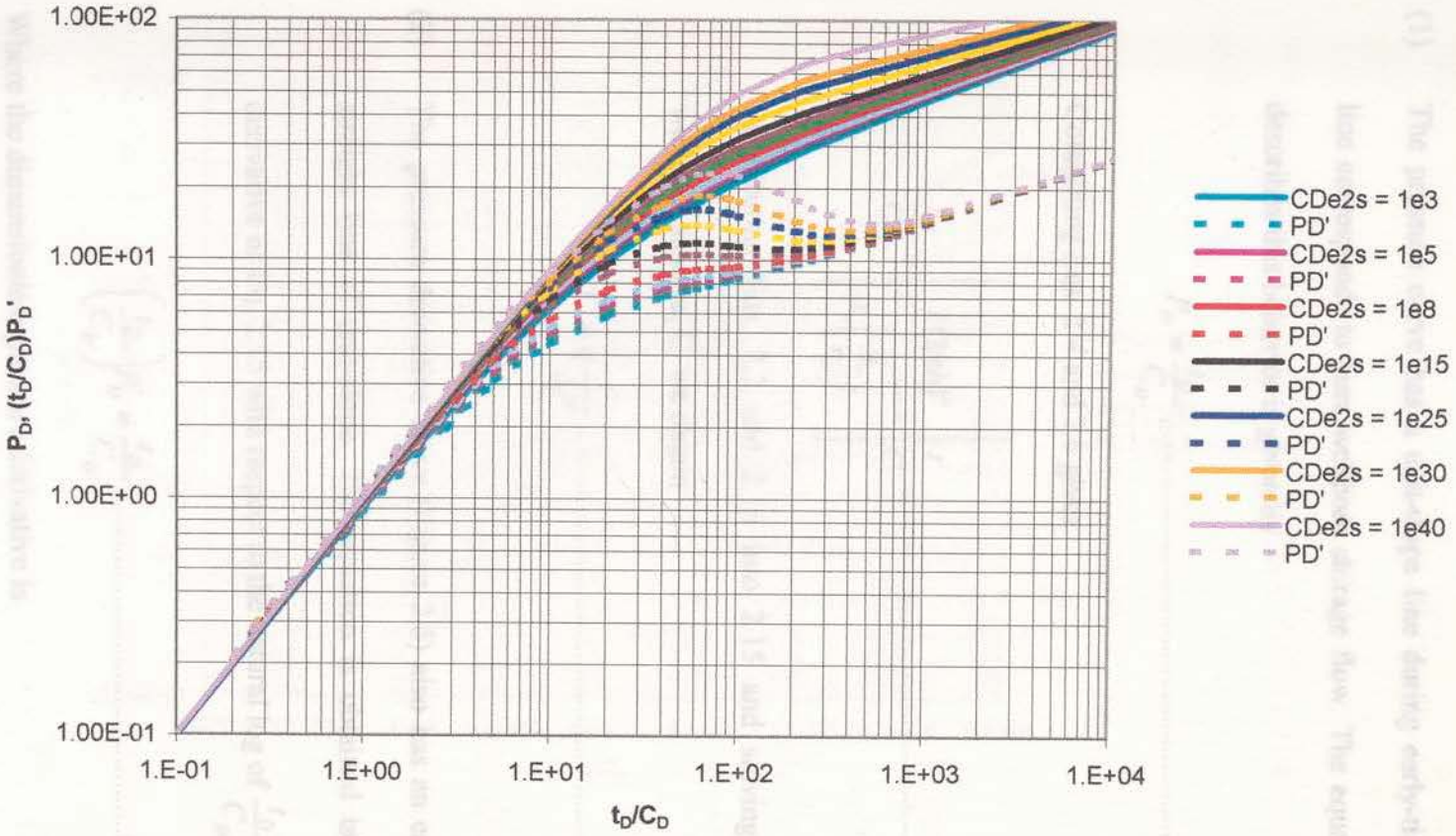

Figure 2.5 - Pressure and Pressure derivative curves for flow behavior index, n = 0.2

(1) The pressure curve has a unit-slope line during early-time. This line corresponds to pure wellbore storage flow. The equation that describes this behavior is given by

$$P_D = \frac{t_D}{C_D} \quad \text{.....(2.15)}$$

Combining Eqs. 2.4 and 2.6 gives

$$\frac{t_D}{C_D} = \left[\frac{k(2\pi h)^n}{\mu_e \left(\frac{q}{r_w} \right)^{n-1}} \right] \frac{t}{C} \quad \text{.....(2.16)}$$

Substituting Eqs. 2.2 and 2.16 into 2.15 and solving for the wellbore storage, C, we obtain

$$C = q \frac{t}{\Delta P} \quad \text{.....(2.17)}$$

(2) The pressure derivative curve (Figure 2.6) also has an early-time straight line of unit-slope. The equation is obtained taking the derivative of Eq. 2.15 with respect to the natural log of $\frac{t_D}{C_D}$.

$$\left(\frac{t_D}{C_D} \right) P_D' = \frac{t_D}{C_D} \quad \text{.....(2.18)}$$

Where the dimensionless pressure derivative is

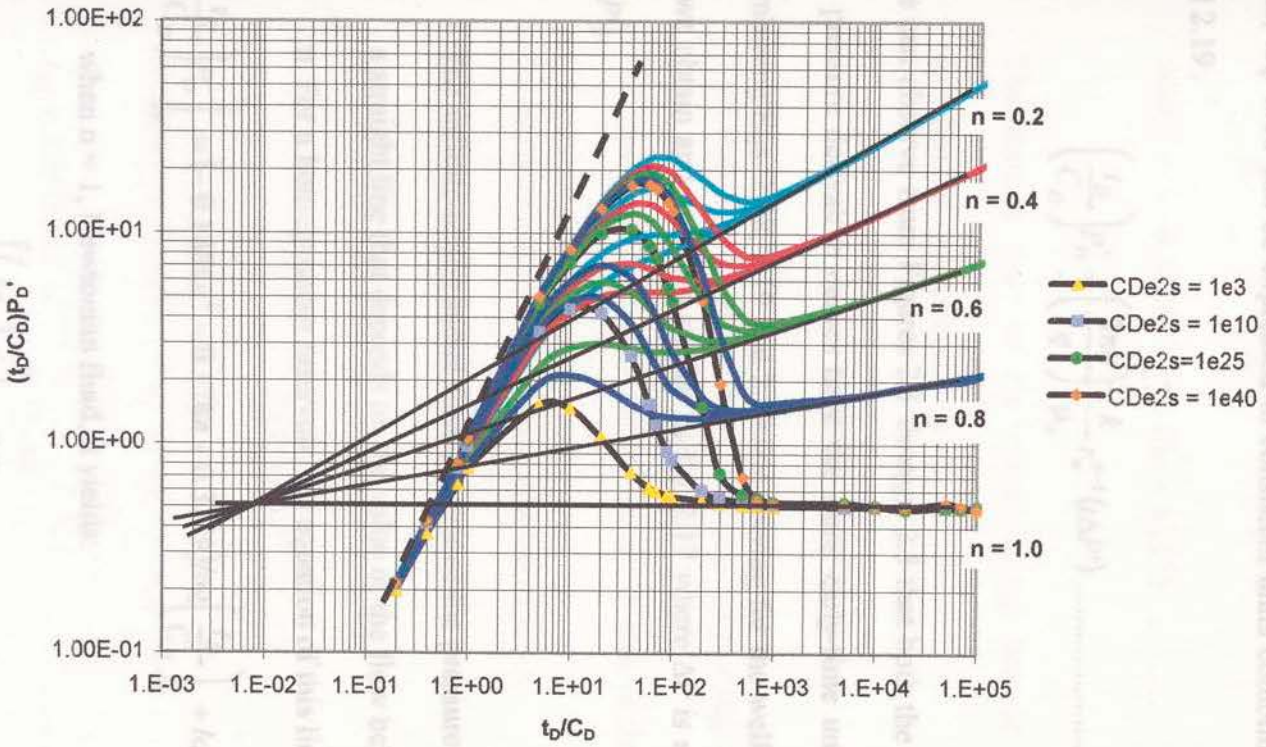

Figure 2.6 - Pressure derivative curves for different flow behavior index, n

$$P_D' = \frac{r_w^2 n \phi c_t 2\pi h}{q} \Delta P' \quad \text{.....(2.19)}$$

Thus, Eq. 2.18 can be expressed in consistent units combining Eqs. 2.16 and 2.19

$$\left(\frac{t_D}{C_D}\right) P_D' = \left(\frac{2\pi h}{q}\right)^n \frac{k}{\mu_e} r_w^{n-1} \left(t\Delta P'\right) \quad \text{.....(2.20)}$$

One can observe from Figures 2.1 through 2.5 that both the pressure and the pressure derivative curves have the same early-time unit slope line. Combining Eqs. 2.18, 2.19 and 2.20 and solving for the wellbore storage, C, we obtain and equation similar to Eq. 2.17 where ΔP is replaced with $\left(t\Delta P'\right)$.

(3) The infinite-acting radial flow portion of the pressure derivative is a straight line that depends on the value of the flow behavior index, n. For a homogeneous reservoir, the equation of this line is:

$$log\left[\left(\frac{t_D}{C_D}\right) P_D'\right]_r = \left(-0.1486n^2 - 0.178n + 0.3279\right) log\left(\frac{t_D}{C_D}\right)_r + log\, 0.5 \quad \text{..(2.21)}$$

when n = 1, Newtonian fluid, it yields:

$$\left[\left(\frac{t_D}{C_D}\right) P_D'\right]_r = 0.5 \quad \text{.....(2.22)}$$

Combining Eqs. 2.20 and 2.21 and solving for the mobility yields:

$$\frac{k}{\mu_e} = \left[0.5 \frac{t_r^{\alpha}}{C^{\alpha}\left(t\Delta P'\right)_r} \frac{(2\pi h)^{n(\alpha-1)} r_w^{(1-n)(1-\alpha)}}{q^{n(\alpha-1)-\alpha}} \right]^{\frac{1}{1-\alpha}} \quad \text{.....(2.23)}$$

where $\alpha = -0.1486n^2 - 0.178n + 0.3279$ .....(2.24)

(4) The starting time of the infinite-acting line of the pressure derivative is approximately given by:

$$\left(\frac{t_D}{C_D}\right)_{SR} = 9.5689x10^4 n^{2.932} \quad \text{.....(2.25)}$$

This equation (Figure 2.7) is obtained by plotting the values of $\frac{t_D}{C_D}$ corresponding to the first point at the start of the straight line for the different values of flow behavior index, n.

Eq. 2.25 is in good agreement with the one obtained by Ikoku and Ramey[18,20]

$$\left(\frac{t_D}{C_D}\right)_{SR} \approx 9.82x10^4 n^{2.7} \quad \text{.....(2.26)}$$

Substituting C_D and t_D and solving for t_{SR} gives:

$$t_{SR} = 9.5689x10^4 n^{2.932} \frac{\mu_e}{k} \frac{C}{(2\pi h)^n} \left(\frac{q}{r_w}\right)^{n-1} \quad \text{.....(2.27)}$$

Where t_{SR} is the starting time of the infinite-acting radial flow line.

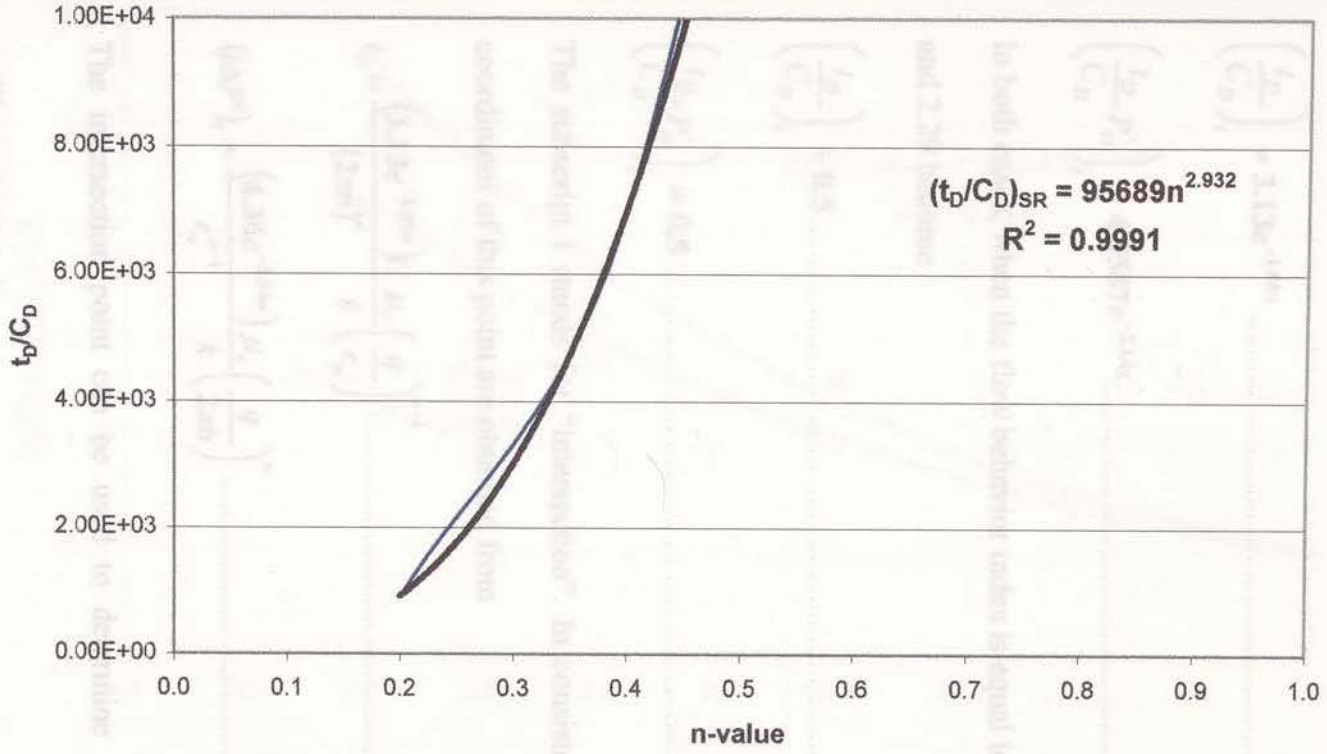

Figure 2.7 -Starting time of the infinite-acting radial flow line for different n values

(5) The early-time unit slope line and the late-time infinite-acting radial flow line of the pressure derivative, intersect at (Figure 2.8):

$$\left(\frac{t_D}{C_D}\right)_i = \mathbf{3.13}e^{-\mathbf{1.85}n} \quad \text{.....(2.28)}$$

$$\left(\frac{t_D}{C_D}P_D'\right)_i = \mathbf{4.3587}e^{-\mathbf{2.14}n} \quad \text{.....(2.29)}$$

In both cases, when the flow behavior index is equal to 1, Eqs. 2.28 and 2.29 become

$$\left(\frac{t_D}{C_D}\right)_i = \mathbf{0.5} \quad \text{.....(2.30)}$$

$$\left(\frac{t_D}{C_D}P_D'\right)_i = \mathbf{0.5} \quad \text{.....(2.31)}$$

The subscript i stands for "intersection". In consistent units, the coordinates of this point are obtained from

$$t_i = \frac{\left(\mathbf{3.13}e^{-\mathbf{1.85}n}\right)C}{(2\pi h)^n}\frac{\mu_e}{k}\left(\frac{q}{r_w}\right)^{n-1} \quad \text{.....(2.32)}$$

$$(t\Delta P')_i = \frac{\left(\mathbf{4.36}e^{-\mathbf{2.14}n}\right)}{r_w^{n-1}}\frac{\mu_e}{k}\left(\frac{q}{2\pi h}\right)^n \quad \text{.....(2.33)}$$

The intersection point can be used to determine $\frac{k}{\mu_e}$ and the wellbore storage, C.

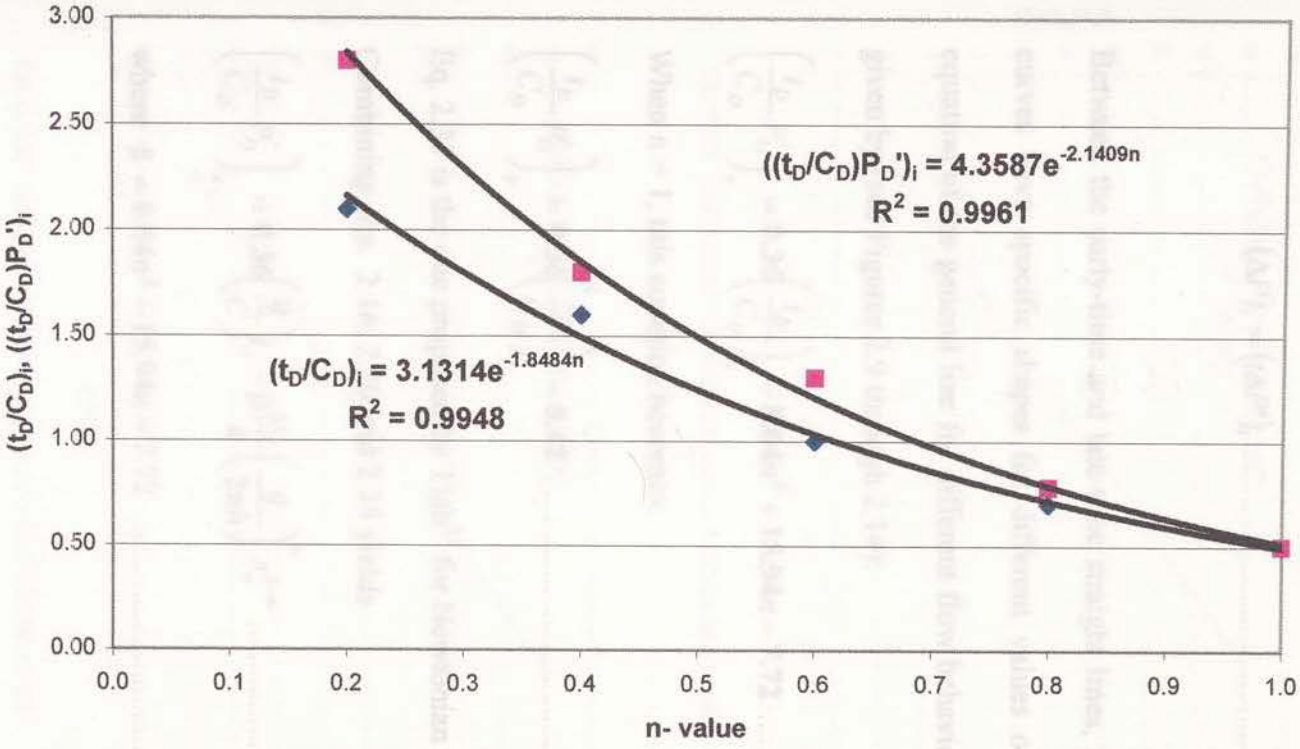

Figure 2.8 - Relationship of Intersection points with the unit-slope line and different n values

Since the unit slope line is the same for pressure and pressure derivative curves, at the intersection point we have:

$$(\Delta P)_i = (t\Delta P')_i \quad \text{.....(2.34)}$$

(6) Between the early-time and late-time straight lines, the derivative curves have specific shapes for different values of C_De^{2S}. The equation of the general line for different flow behavior index, n, is given by (see Figures 2.9 through 2.14):

$$\left(\frac{t_D}{C_D}P_D'\right)_x = \mathbf{0.36}\left(\frac{t_D}{C_D}\right)_x - \mathbf{8.64}n^2 + \mathbf{15.94}n - \mathbf{7.72} \quad \text{.....(2.35)}$$

When n = 1, this equation becomes:

$$\left(\frac{t_D}{C_D}P_D'\right)_x = \mathbf{0.36}\left(\frac{t_D}{C_D}\right)_x - \mathbf{0.42} \quad \text{.....(2.36)}$$

Eq. 2.35 is the one proposed by Tiab[31] for Newtonian case.

Combining eqs. 2.16, 2.20 and 2.35 yields

$$\left(\frac{t_D}{C_D}P_D'\right)_x = \mathbf{0.36}\left(\frac{q}{C}\right)t_x - \beta\frac{\mu_e}{k}\left(\frac{q}{2\pi h}\right)^n r_w^{1-n} \quad \text{.....(2.37)}$$

where $\beta = 8.64n^2 - 15.94n + 7.72$ .....(2.38)

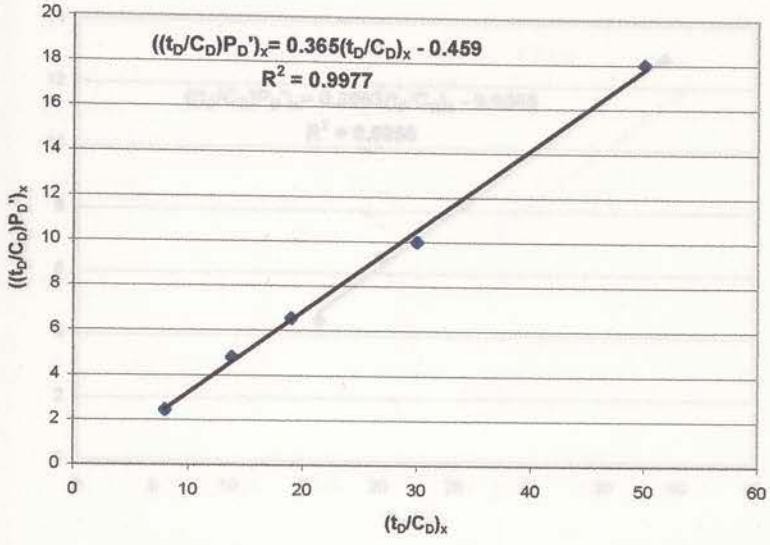

Figure 2.9 - Correlation of the maximum point coordinates for n = 1.0

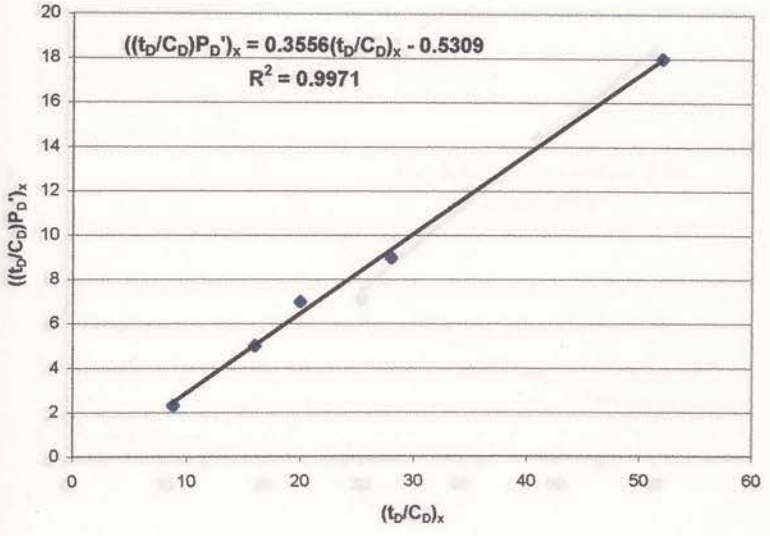

Figure 2.10 - Correlation of the maximum point coordinates for n = 0.8

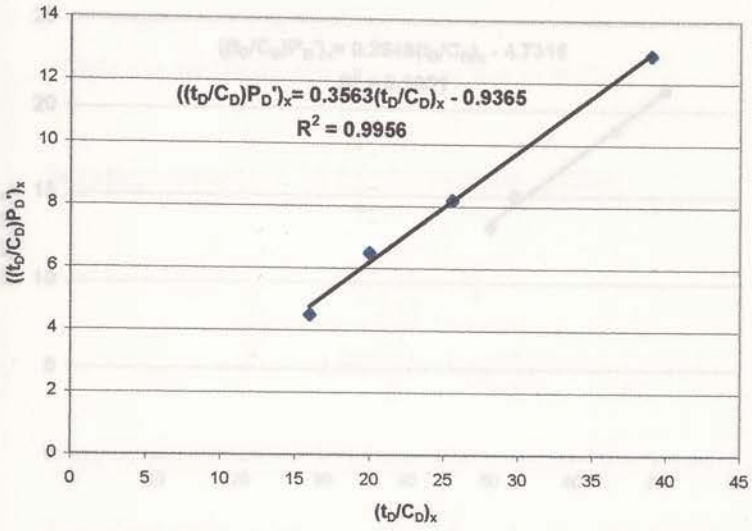

Figure 2.11 - Correlation of the maximum point coordinates for n = 0.6

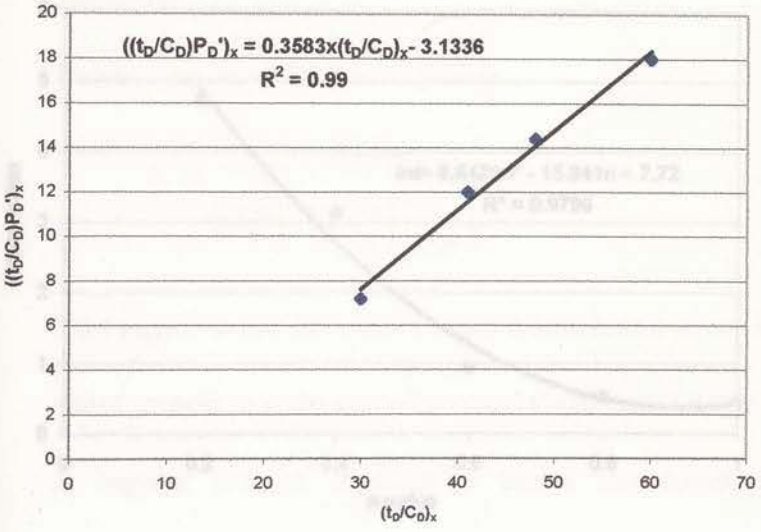

Figure 2.12 - Correlation of the maximum point coordinates for n = 0.4

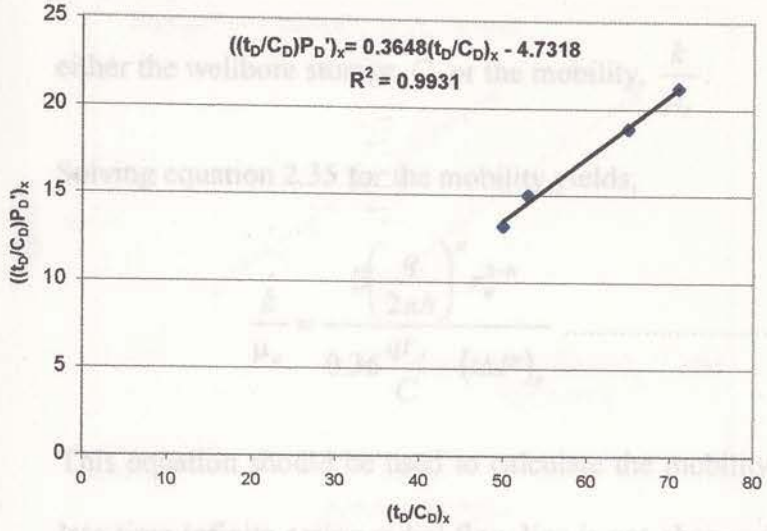

Figure 2.13 - Correlation of the maximum point coordinates for n = 0.2

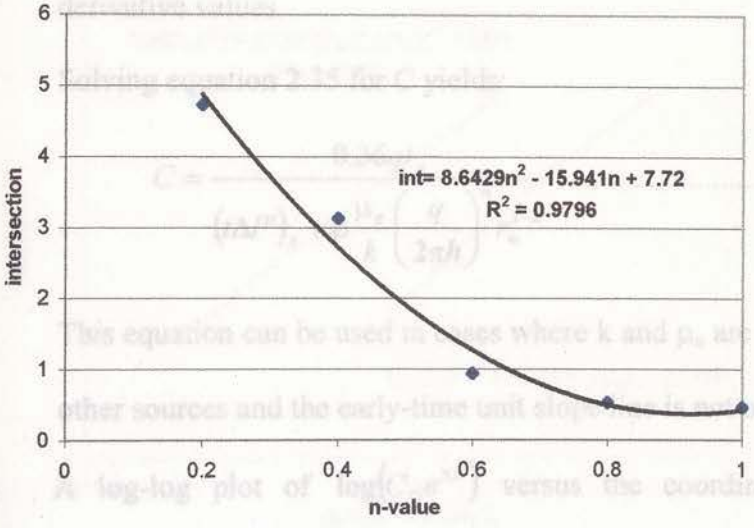

Figure 2.14 - General relationship of maximum points and flow behavior indexes, n

and $(t\Delta P')_x$ and t_x are the coordinates of the maximum point of the pressure derivative curve. From equation 2.35, one can calculate either the wellbore storage, C, or the mobility, $\frac{k}{\mu_e}$.

Solving equation 2.35 for the mobility yields;

$$\frac{k}{\mu_e} = \frac{\beta\left(\frac{q}{2\pi h}\right)^n r_w^{1-n}}{0.36\frac{qt_x}{C} - (t\Delta P')_x} \quad \text{.....(2.39)}$$

This equation should be used to calculate the mobility only if the late-time infinite-acting radial flow line is not observed, such as in a short test, or when there is too much noise in the late-time derivative values.

Solving equation 2.35 for C yields:

$$C = \frac{0.36qt_x}{(t\Delta P')_x + \beta\frac{\mu_e}{k}\left(\frac{q}{2\pi h}\right)^n r_w^{1-n}} \quad \text{.....(2.40)}$$

This equation can be used in cases where k and μ_e are known from other sources and the early-time unit slope line is not observed.

(7) A log-log plot of $\log(C_D e^{2S})$ versus the coordinates of the maximum points yields the following equations (see Figures 2.15 through 2.20):

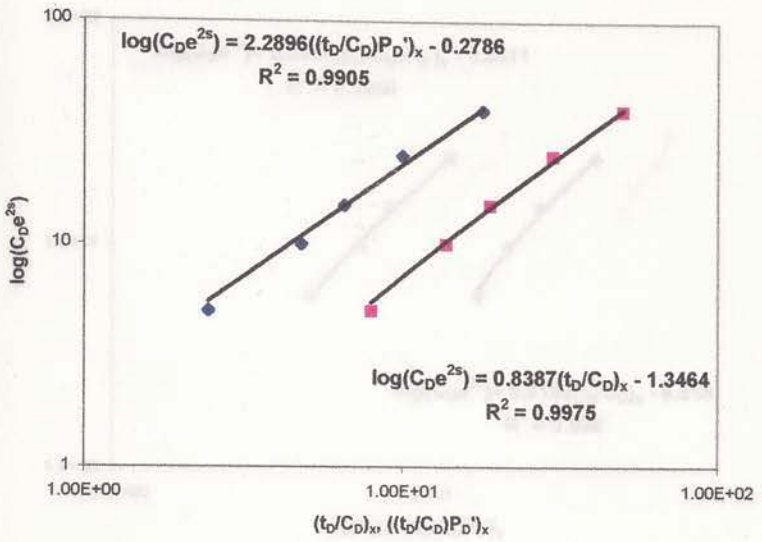

Figure 2.15 -Relationship of Log(C_De^{2S}) and the coordinates of maximum points for n = 1.0

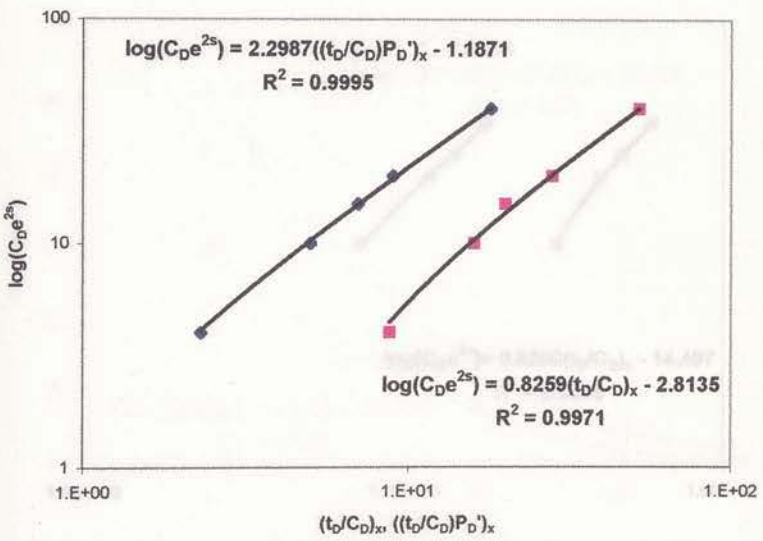

Figure 2.16 - Relationship of Log(C_De^{2S}) and the coordinates of maximum points for n = 0.8

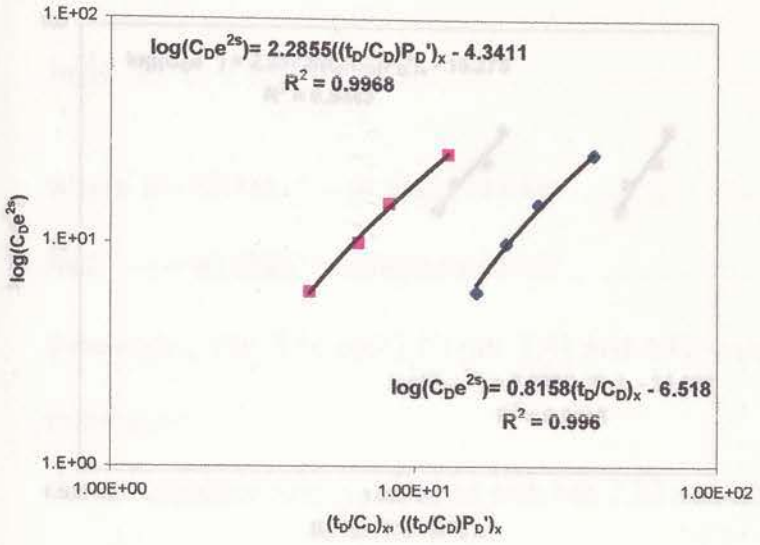

Figure 2.17 - Relationship of Log(C_De^{2S}) and the coordinates of the maximum points for n = 0.6

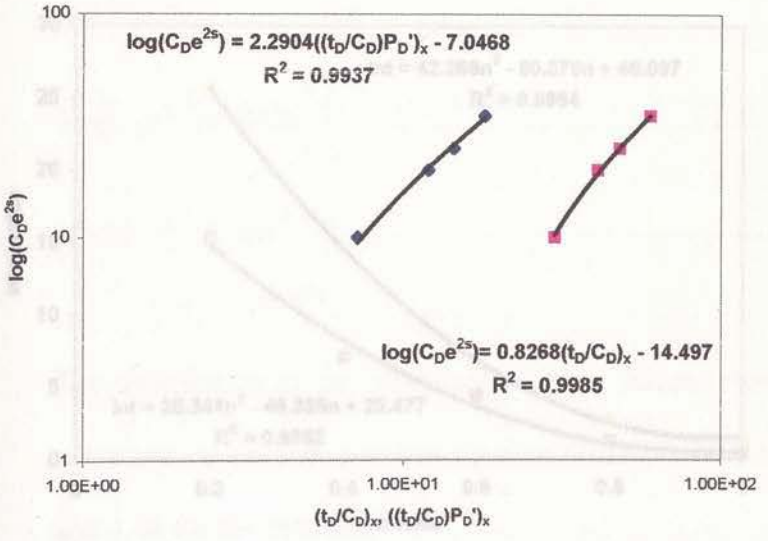

Figure 2.18 - Relationship of Log(C_De^{2S}) and the coordinates of the maximum points for n = 0.4

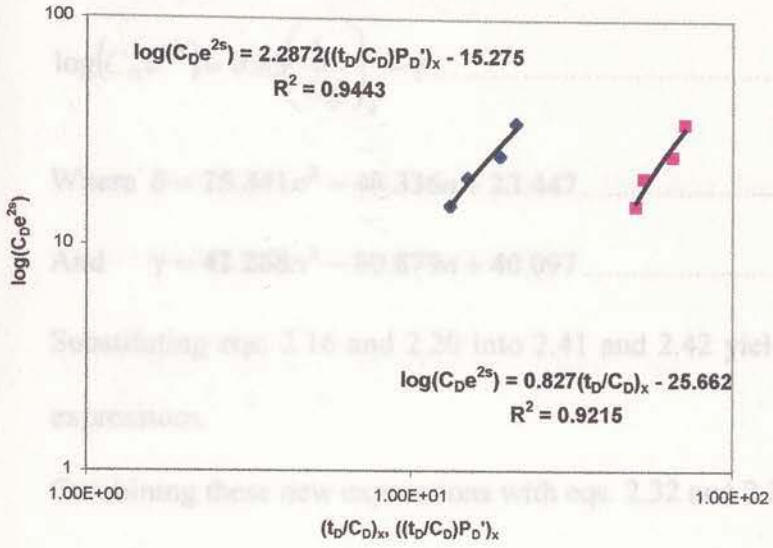

Figure 2.19 - Relationship of $Log(C_De^{2S})$ and the coordinates of the maximum points for n = 0.2

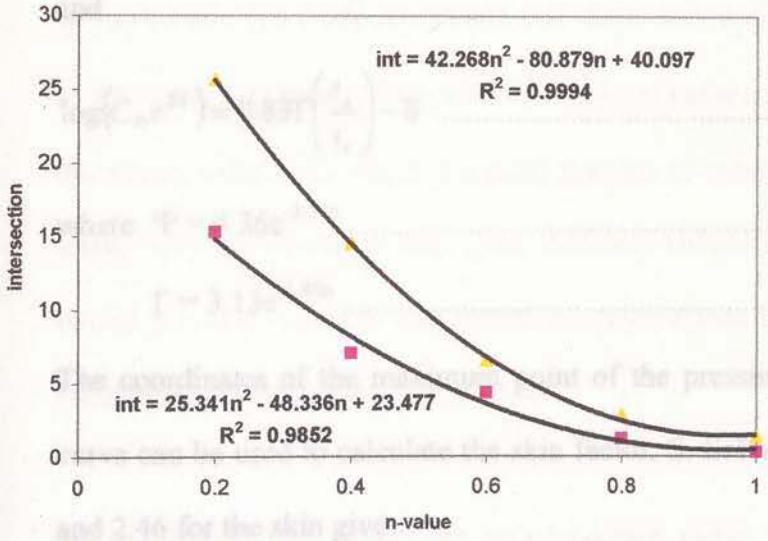

Figure 2.20 - Values of intersection points for different flow behavior indexes in equations (2.41) and (2.42)

$$\log\left(C_D e^{2S}\right) = \mathbf{2.29}\left(\frac{t_D}{C_D}P_D'\right)_x - \delta \quad \text{.....(2.41)}$$

$$\log\left(C_D e^{2S}\right) = \mathbf{0.83}\left(\frac{t_D}{C_D}\right)_x - \gamma \quad \text{.....(2.42)}$$

Where $\delta = \mathbf{25.341}n^2 - \mathbf{48.336}n + \mathbf{23.447}$ .....(2.43)

And $\gamma = \mathbf{42.268}n^2 - \mathbf{80.879}n + \mathbf{40.097}$ .....(2.44)

Substituting eqs. 2.16 and 2.20 into 2.41 and 2.42 yields two new expressions.

Combining these new expressions with eqs. 2.32 and 2.33 gives:

$$\log\left(C_D e^{2S}\right) = \mathbf{2.29}\Psi\left(\frac{(t\Delta P')_x}{(t\Delta P')_i}\right) - \delta \quad \text{.....(2.45)}$$

and

$$\log\left(C_D e^{2S}\right) = \mathbf{0.83}\Gamma\left(\frac{t_x}{t_i}\right) - \delta \quad \text{.....(2.46)}$$

where $\Psi = 4.36e^{-2.14n}$ .....(2.47)

$\Gamma = 3.13e^{-1.85n}$ .....(2.48)

The coordinates of the maximum point of the pressure derivative curve can be used to calculate the skin factor, S. Solving eqs. 2.45 and 2.46 for the skin give:

$$S = \frac{\mathbf{1}}{\mathbf{2}}\left[\mathbf{5.27}\Psi\frac{(t\Delta P')_x}{(t\Delta P')i} - \mathbf{2.303}\delta - \ln\left(C_D\right)\right] \quad \text{.....(2.49)}$$

and

$$S = \frac{1}{2}\left[1.91\Gamma\frac{t_x}{t_i} - 2.303\gamma - \ln(C_D)\right] \quad \text{.....(2.50)}$$

If the unit-slope line is not defined, the skin factor can be calculated using the following equations:

$$S = \frac{1}{2}\left[5.27\left(\frac{2\pi h}{q}\right)^n \frac{k}{\mu_e} r_w^{n-1}(t\Delta P')_x - 2.303\delta - \ln(C_D)\right] \quad \text{.....(2.51)}$$

and

$$S = \frac{1}{2}\left[1.91(2\pi h)^n \frac{k}{\mu_e}\left(\frac{r_w}{q}\right)^{n-1}\frac{t_x}{C} - 2.303\gamma - \ln(C_D)\right] \quad \text{.....(2.52)}$$

In some cases the wellbore storage bell shape may appear to be flat at the maximum point. One can read the right value of $(t\Delta P')_x$ but the wrong value of t_x. So, it is a good practice to calculate the skin using both equations. If they give different values of skin then obtain a new value of t_x and repeat the calculations until the two equations give the same value of skin.

(8) An expression that relates the infinite-acting radial flow regime with the maximum points for different values of C_De^{2S} can be derived by dividing equation (2.35) with (2.21):

$$\frac{\left(\frac{t_D}{C_D}P_D'\right)_x}{\left(\frac{t_D}{C_D}P_D'\right)_r} = \frac{0.36\left(\frac{t_D}{C_D}\right)_x - \beta}{0.5\left(\frac{t_D}{C_D}\right)_r^{\alpha}} \quad \text{.....(2.53)}$$

Using eqs. 2.16, 2.20 with equation 2.53 gives

$$\frac{(t\Delta P')_x}{(t\Delta P')_r} = 2\left[0.36\left(\frac{k}{\mu_e}\right)^{1-\alpha} \frac{(2\pi h)^{n(1-\alpha)}}{C^{1-\alpha}\left(\frac{q}{r_w}\right)^{(n-1)(1-\alpha)}} \frac{t_x}{t_r^{\alpha}} - \beta \frac{C^{\alpha}\left(\frac{q}{r_w}\right)^{(n-1)\alpha}}{(2\pi h)^{n\alpha} t^{\alpha}}\right] \quad \text{.....(2.54)}$$

For n = 1 this equation reduces to

$$\frac{(t\Delta P')_x}{(t\Delta P')_r} = 2\left[0.36\left(\frac{k}{\mu_e}\right)\frac{(2\pi h)}{C}t_x - \beta\right] \quad \text{.....(2.55)}$$

Where β = 0.42. That is the equation proposed by Tiab[31] for Newtonian case.

Equation 2.54 can be used to verify either the mobility, $\frac{k}{\mu_e}$, or the wellbore storage coefficient, C.

2.1.3) Procedures

Case 1 (base case) – Unit-slope and infinite-acting lines are observed

The following step-by-step procedure is for a general case where the early-time unit-slope line and the late time infinite-acting radial flow line have definitely been observed, and are well defined.

Step 1. - Plot ΔP and $(t\Delta P')$ versus time on a log-log graph.

Step 2. - Draw the unit-slope line corresponding to the wellbore storage flow regime using early-time pressure and pressure derivative points.

Step 3. - Draw the infinite-acting radial flow line using late-time pressure derivative points. Find the slope and read the value of n from Figure 2.21

Step 4. - Read the coordinates of the maximum point on the pressure derivative curve: t_x and $(t\Delta P')_x$

Step 5. - Read the coordinates of the point where the unit-slope line and the infinite-acting radial line intersect: t_i and ΔP_i.

Step 6. - Calculate the wellbore storage coefficient, C from equation 2.17

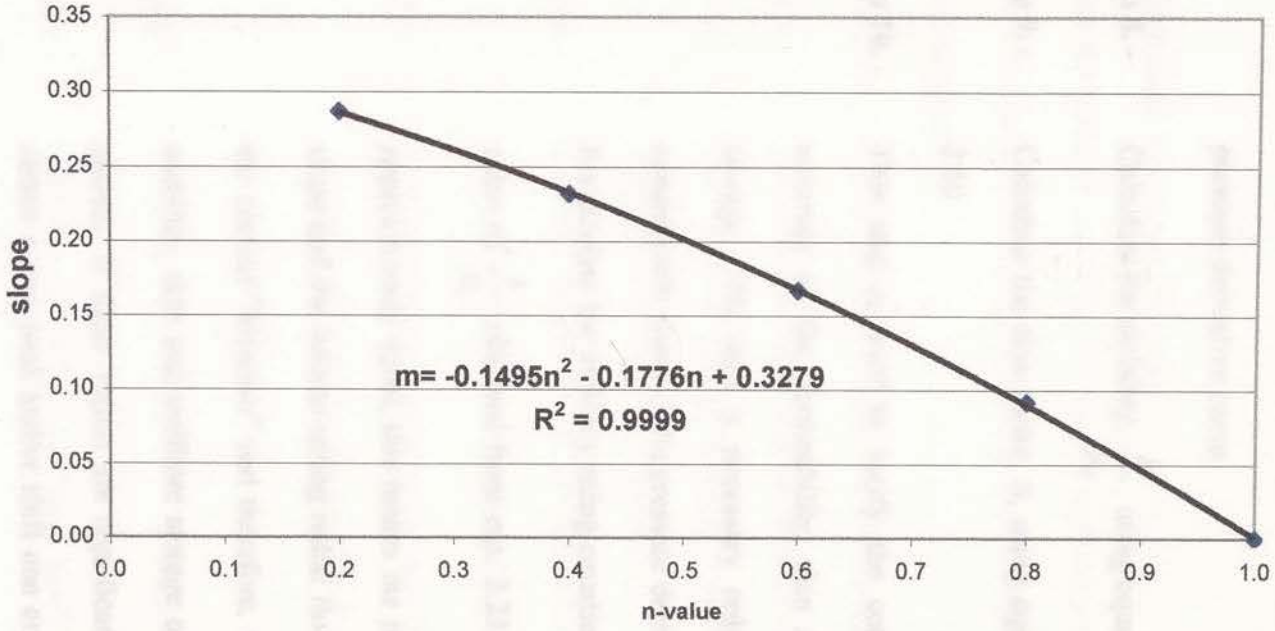

Figure 2.21 - Relationship between the slope of the infinite-acting radial flow line and the flow behavior index, n

Step 7. - Read any convenient time, t_r, during the infinite-acting radial flow line and read the $(t\Delta P')_r$ from the pressure derivative curve.

Step 8. - Calculate the mobility, $\frac{k}{\mu_e}$, using equation 2.23

Step 9. - Calculate the skin factor, S, using eqs. 2.49 or/and 2.50

Step 10. - This step is used to verify the correctness and accuracy of the permeability, skin and wellbore storage. This step is necessary only if there is considerable noise in the pressure derivative values. Recalculate the mobility using equation 2.54. If the value of $\frac{k}{\mu_e}$ obtained from eqs. 2.23 and 2.54 are approximately equal, this means the peak, the unit-slope and the infinite-acting radial flow lines are in the correct "location" and therefore, the values of mobility, skin and wellbore storage coefficient are correct. If these values are significantly different, obtain a new peak and/or shift one or both straight

lines and repeat steps 3 through 9 until obtain similar values of mobility.

Case 2 – Unit-slope line is not observed

When the pressure test does not have enough early-time points to draw the unit-slope line, the following step-by-step procedure is recommended.

Step 1. - Plot ΔP and $(t\Delta P')$ versus time on a log-log graph.

Step 2. - Draw the infinite-acting radial flow line using late-time pressure derivative points. Find the slope and read the value of n from Figure 2.21

Step 3. - Read the coordinates of the maximum point on the pressure derivative curve: t_x and $(t\Delta P')_x$

Step 4. - Read any convenient time, t_r, during the infinite-acting radial flow line and read the $(t\Delta P')_r$ from the pressure derivative curve.

Step 5. - Calculate the mobility, $\frac{k}{\mu_e}$, using equation 2.23

Step 6. - Calculate the wellbore storage coefficient, C from equation 2.40

Step 7. - Calculate the skin factor, S, using eqs. 2.51 or/and 2.52

Case 3 – The infinite-acting radial flow line is not observed

If the pressure test is too short to observe the infinite-acting radial flow line, or there is too much scatter in the late-time derivative points or the boundary effects are felt before the infinite-acting flow regime is fully developed, then the following step-by-step procedure is recommended. In this case the flow behavior index, n, should be known from other source such as laboratory experiments.

Step 1. - Plot ΔP and $(t\Delta P')$ versus time on a log-log graph.

Step 2. - Draw the unit-slope line corresponding to the wellbore storage flow regime using early-time pressure and pressure derivative points.

Step 3. - Read the coordinates of the maximum point on the pressure derivative curve: t_x and $(t\Delta P')_x$

Step 4. - Calculate the wellbore storage coefficient, C from equation 2.17

Step 5. - Calculate the mobility, $\frac{k}{\mu_e}$, using equation 2.39

Step 6. - Calculate the coordinates of the points of intersection of the unit-slope line and the infinite-acting radial flow line (had the test been run long enough to observe it) from eqs. 2.32 and 2.33

Step 7. - Calculate the skin factor, S, using eqs. 2.49 or/and 2.50

Step 8. - Recalculate $\frac{k}{\mu_e}$ from equation 2.54. If the two values of $\frac{k}{\mu_e}$ obtained in step 5 and 8 are similar, then k, s and C are correct. If not, obtain a new peak and/or shift the unit-slope line and repeat the process until the two values of $\frac{k}{\mu_e}$ are similar. If needed, the infinite-acting radial flow line can now be drawn.

Case 4 – The unit-slope line and the peak are not observed

In some pressure test, the first pressure reading occurred well after the end of wellbore storage flow regime, such as that the peak of the pressure derivative is not observed. The following step-by-step procedure is recommended.

Step 1. - Plot ΔP and $(t\Delta P')$ versus time on a log-log graph.

Step 2. - Draw the infinite-acting radial flow line using late-time pressure derivative points. Find the slope and read the value of n from Figure 2.21

Step 3. - Read any convenient time, t_r, during the infinite-acting radial flow line and read the $(t\Delta P')_r$ from the pressure derivative curve.

Step 4. - Calculate the mobility, $\frac{k}{\mu_e}$, using equation 2.23

Step 5. - Determine from the graph the starting time of the infinite-acting radial flow line, t_{SR}, of the pressure derivative curve.

Step 6. - Calculate the wellbore storage coefficient, C, using equation 2.27

Step 7. - Plot ΔP versus $t^{\frac{1-n}{3-n}}$ in Cartesian coordinates. A straight line is obtained. From it extrapolate the line and find the value of ΔP when t = 0 seconds. Using the analytical inversion for the long-time approximation of equation 2.10, evaluated it at t = 0 seconds and $\Delta P = \Delta P_o$, the skin factor can be

calculated. The equation is given by Ikoku and Ramey[18] as:

$$S = \left(\frac{\Delta P_o}{r_w^{1-n}}\right)\left(\frac{2\pi h}{q}\right)^n \frac{k}{\mu_e} + \frac{1}{1-n} \quad \text{.....(2.56)}$$

Case 5 – The unit-slope and the infinite-acting radial flow line are not observed

In some short tests, both the unit-slope line and the infinite-acting radial flow lines are missing. In this case if the wellbore storage coefficient, C, and the flow behavior index can be known from completion data and laboratory experiments, respectively, then the following procedure is recommended.

Step 1. - Plot ΔP and $(t\Delta P')$ versus time on a log-log graph.

Step 2. - Estimate the wellbore storage coefficient, C, from well completion data, For a wellbore with changing liquid level $C = 144\frac{V_u}{\rho}$ where V_u is the wellbore volume per unit length. When the wellbore is completely filled with a single-phase fluid $C = c_w V_w$, where V_w is the total wellbore volume

and c_w is the compressibility of the fluid in the wellbore.

Step 3. - Read the coordinates of the maximum point on the pressure derivative curve: t_x and $(t\Delta P')_x$

Step 4. - Calculate the mobility, $\frac{k}{\mu_e}$, using equation 2.39

Step 5. - Calculate the coordinates of the points of intersection of the unit-slope line and the infinite-acting radial flow line (had the test been run long enough to observe it) from eqs. 2.32 and 2.33

Step 6. - Calculate the skin factor, S, using eqs. 2.49 or/and 2.50

If the permeability is known from other sources then calculate C from equation 2.40 and the skin factor as discussed in step 5 and 6 (case 5).

2.1.4) Application

A pressure falloff test[33] in a reservoir that is influenced by skin and wellbore storage has a simulated pressure data as a function of time listed in table 2.1. Other reservoir and well data are:

Wellbore radius:	0.2 ft
Reservoir thickness:	50 ft
Porosity:	0.2
Total compressibility:	1.45×10^{-5} psi^{-1}
Injection rate:	200 STB/D
Formation Volume Factor:	1 RB/STB

Calculate the permeability-viscosity ratio, skin factor and wellbore storage coefficient.

Table 2.1 Pressure and Pressure derivative for falloff test

Δt, sec	ΔP, Kpa	tP', kpa
1.44	4.89E+01	
1.98	6.60E+01	6.24E+01
2.7	8.80E+01	8.10E+01
3.6	1.14E+02	1.03E+02
4.68	1.44E+02	1.27E+02
5.76	1.73E+02	1.49E+02
7.2	2.09E+02	1.74E+02
8.64	2.42E+02	1.97E+02
1.01E+01	2.74E+02	2.18E+02
1.44E+01	3.61E+02	2.68E+02
1.98E+01	4.53E+02	3.13E+02
2.70E+01	5.57E+02	3.56E+02
3.60E+01	6.65E+02	3.91E+02
4.68E+01	7.72E+02	4.20E+02
5.76E+01	8.61E+02	4.41E+02
7.20E+01	9.62E+02	4.60E+02
8.64E+01	1.05E+03	4.70E+02
1.01E+02	1.12E+03	4.76E+02
1.44E+02	1.29E+03	4.85E+02
1.98E+02	1.45E+03	4.87E+02
2.70E+02	1.60E+03	4.92E+02
3.60E+02	1.74E+03	4.94E+02
4.68E+02	1.87E+03	4.97E+02
5.76E+02	1.97E+03	5.06E+02
7.20E+02	2.09E+03	5.13E+02
8.64E+02	2.18E+03	5.21E+02
1.01E+03	2.26E+03	5.28E+02
1.44E+03	2.45E+03	5.42E+02
1.98E+03	2.63E+03	5.60E+02
2.70E+03	2.81E+03	5.85E+02
3.60E+03	2.98E+03	6.08E+02
4.68E+03	3.14E+03	6.36E+02
5.76E+03	3.27E+03	6.61E+02
7.20E+03	3.42E+03	6.86E+02
8.64E+03	3.55E+03	7.09E+02
1.01E+04	3.66E+03	7.28E+02
1.44E+04	3.93E+03	7.68E+02
1.98E+04	4.18E+03	8.12E+02
2.70E+04	4.44E+03	8.63E+02
3.60E+04	4.69E+03	9.09E+02
4.68E+04	4.94E+03	9.85E+02
5.70E+04	5.14E+03	1.01E+03
7.20E+04	5.37E+03	1.03E+03
8.64E+04	5.56E+03	1.09E+03
1.01E+05	5.73E+03	1.12E+03
1.44E+05	6.14E+03	

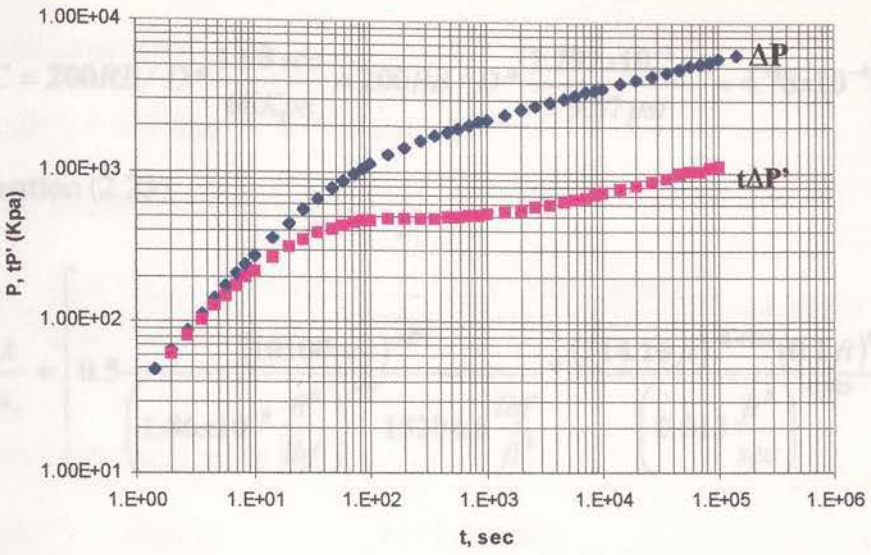

Figure 2.22. Example of falloff test

Figure 2.22 is a log-log plot of ΔP and $(t\Delta P')$ versus time. Reading the value of the slope of the infinite-acting radial flow line, we obtain:

$$m = \frac{\log(1.12x10^3) - \log(7.28x10^2)}{\log(1.01x10^5) - \log(1.01x10^4)} = 0.187$$

Using Figure 2.21 we can obtain the flow behavior index, n. From this slope,

$$n = 0.544$$

Reading from Figure 2.22, we obtain the following information;

$T_i = 5$ sec $\quad \Delta P_i = (t\Delta P')_i = 150Kpa \quad t_{USL} = 1.98$ sec $\quad \Delta P_{USL} = 66Kpa$

$T_x = 75$ sec $\quad (t\Delta P')_x = 490Kpa \quad (t\Delta P')_r = 728Kpa \quad t_r = 10100$sec

From equation (2.17), we can obtain the wellbore storage coefficient

$$C = 200RB/D * \frac{1.98\,sec}{66Kpa} = 200RB/D * \frac{2.292x10^{-5}D}{9.57\,psi} = 4.78x10^{-4}\left[\frac{RB}{psi}\right]$$

From equation (2.23)

$$\frac{k}{\mu_e} = \left[0.5\frac{(10100\,sec)^{187}}{\left(1.86x10^{-5}\frac{ft^5}{lbf}\right)^{.187}\,15204.6\frac{lbf}{ft^2}} * \frac{(314.16\,ft)^{-0.4423}(0.2\,ft)^{0.3707}}{\left(0.013\frac{ft^3}{sec}\right)^{-0.629}}\right]^{\frac{1}{0.813}}$$

$$\frac{k}{\mu_e} = 2.28x10^{-7}\left[\frac{ft^{3.544}}{lb_f\,sec^{0.544}}\right]$$

Using equation (2.6), we can calculate the dimensionless wellbore storage, C_D,

$$C_D = \frac{4.78x10^{-4}RB/psi}{2\pi 50\,ft * 0.2 * 1.45x10^{-5}\,psi^{-1} * 0.544 * (0.2\,ft)^2} = 135.4$$

From equation (2.49) and (2.50) we can calculate the skin factor, S.

$$S = \frac{1}{2}\left[7.17 * \frac{490Kpa}{150Kpa} - 2.303 * 4.54 - ln(135.4)\right] = 4.03$$

$$S = \frac{1}{2}\left[2.19 * \frac{75\,sec}{5\,sec} - 2.303 * 8.61 - ln(135.4)\right] = 4.06$$

"Well is damaged"

Analyzing the pressure test using a Newtonian model, the reservoir and well parameters are:

$(t\Delta P')_i$ = 500 Kpa t_i = 15 sec

The wellbore storage is given by:

$$C = \left(\frac{qB}{24}\right)\frac{t_{USL}}{\Delta P_{USL}} = \left(\frac{200 STB/D * 1 RB/STB}{24}\right)\frac{0.0042h}{72.52 psi} = 4.83x10^{-4}\left[\frac{RB}{psi}\right]$$

The mobility is given by:

$(t\Delta P')_r$ = 500 Kpa $t_r = 1x10^4$ sec

$$\frac{k}{\mu} = \frac{70.6qB}{h(t\Delta P')_r} = \frac{70.6 * 200 STB/D * 1 RB/STB}{50 ft * 72.52 psi} = 3.89\left[\frac{mD}{cp}\right]$$

$$\frac{k}{\mu} = 1.98x10^{-9}\left[\frac{ft^4}{lb_f\, sec}\right]$$

The skin factor can now be calculated:

$$S = 0.5\left[\frac{\Delta P_r}{(t\Delta P')_r} - ln\left(\frac{kt_r}{\phi\mu c_t r_w^2}\right) + 7.43\right] = 0.5\left[\frac{3800 Kpa}{500 Kpa} - 18.35 + 7.43\right]$$

$S = -1.66$

To verify if all the values are correct, we should calculate the mobility using the following equation knowing that $(t\Delta P')_i = (t\Delta P')_r$

$$\frac{k}{\mu} = 9416.2\frac{C}{ht_x}\left[0.5\frac{(t\Delta P')_x}{(t\Delta P')_r} + 0.42\right]$$

$$\frac{k}{\mu} = 3.97\left[\frac{mD}{cp}\right]$$

"Well is stimulated"

Analysis of the Results:

The values obtained using a Newtonian model to analyze the pressure behavior are very different from those obtained using a non-Newtonian model. The mobility can not be compared because of the difference in the units. The wellbore storage values are pretty similar with an error of ≈1%. In the case of the skin factor, one can observe that with using a Newtonian model the value is negative (well is stimulated) and with a non-Newtonian model the value is positive (well is damaged). This value is the one that gives most of the error and the analyst can overlook this fact.

Table 2.2 Comparison of results

Parameter	Non-Newtonian Model	Newtonian Model[31]	simulated[33]
n	0.544	1.0	0.5
$\frac{k}{\mu_e}$	$2.25\text{x}10^{-7}\left[\frac{ft^{3.544}}{lb_f\, sec^{0.544}}\right]$	$1.98\text{x}10^{-9}\left[\frac{ft^4}{lb_f\, sec}\right]$	$1.52\text{x}10^{-8}$ $\left[\frac{ft^4}{lb_f\, sec}\right]$
C_D	135.4	74.41	100
S	4.03	-1.66	4.00

CHAPTER III

PRESSURE RESPONSE OF NON-NEWTONIAN FLUID IN THE PRESENCE OF A LINEAR BOUNDARY

Linear discontinuities, particularly single sealing faults or the presence of a strong aquifer, have been studied thoroughly[27,34-36]. Figure 3.1 shows a single well near a linear boundary in an otherwise infinite-acting reservoir.

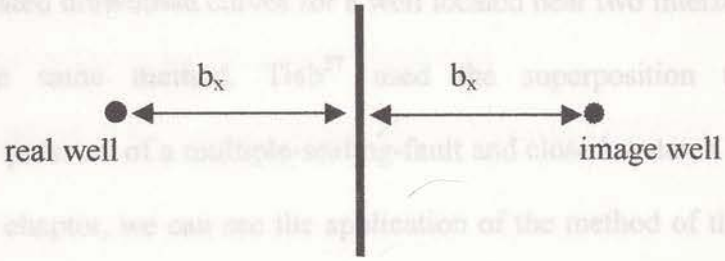

Figure 3.1 - A well near a single linear boundary (Image method)

To obtain the effect of a single linear boundary (sealing fault or a constant pressure), we use the method of images and add an image well as shown in Figure 3.1. The method of the images is a procedure for distributing sources and sinks in an infinite porous medium so that bounding planes that are either no-flow boundaries or constant- pressure boundaries are formed in the porous medium. This method can be applied to sources of any shape. The location of the sources

and sinks (the images) is the same whether the boundary is a no-flow or a constant-pressure boundary.

The first time that this application appears in the petroleum literature was in 1954 when Matthews, Brons and Hazebroek[34] discussed the determination of average reservoir pressures in closed reservoirs systems. They studied reservoirs with non-rectangular drainage shapes such as the triangle, rhombus and hexagon. Horner[3] used the method of images to analyzed pressure transient data in the presence of a single fault. Jones[35] applied it to multiple-sealing-fault systems. Van pollen[36] generated drawdown curves for a well located near two intersecting faults by using the same method. Tiab[27] used the superposition to generate dimensionless pressure of a multiple-sealing-fault and closed systems.

In this chapter, we can see the application of the method of the images to evaluate the pressure behavior of a well in the presence of a single linear boundary for the case of non-Newtonian fluid with the effects of wellbore storage and skin.

3.1) Well located near a single linear Boundary

If the well is near a single linear boundary the image technique yields a image well on the opposite side of the boundary at the same distance b_x as follows: a producing well for the no-flow boundary case, and an injection well for the flow boundary case.

The solution for this case is obtained by use of the method of images.

The dimensionless pressure at the real well is

$$P_D(r_D,t_D)=P_D(r_{Dw},t_D)\pm P_D(r_{DI},t_D) \quad \text{.....(3.1)}$$

where $r_{Dw}=\frac{r_w}{r_w}=1$ .....(3.2)

$$r_{DI}=\frac{2b_x}{r_w} \quad \text{.....(3.3)}$$

b_x is the distance between the real well and the image well as shown in Figure 3.1. The negative sign corresponds to the injection image well and the positive one to the producing image well.

The equation in the Laplace space that describes this behavior is given by

$$\overline{P}_{Dw}(z)=\frac{K_v(\beta\sqrt{z})}{z\left(\sqrt{z}K_\beta(\beta\sqrt{z})+zC_D\left[K_v(\beta\sqrt{z})+S\sqrt{z}K_\beta(\beta\sqrt{z})\right]\right)}$$

$$\pm\frac{(2b_{XD})^{\frac{1-n}{2}}K_v\left(\beta\sqrt{z}(2b_{XD})^{1/\beta}\right)}{z\left(\sqrt{z}K_\beta(\beta\sqrt{z})+zCD\left[(2b_{XD})^{\frac{1-n}{2}}K_v\left(\beta\sqrt{z}(2b_{XD})^{1/\beta}\right)+S\sqrt{z}K_\beta(\beta\sqrt{z})\right]\right)} \quad \text{...(3.5)}$$

where $b_{XD}=\frac{b_x}{r_w}$.

The solution of this equation is obtained by applying numerical inversion as in the case of infinite reservoir.

The behavior of the dimensionless pressure of a single well with wellbore storage and skin near a sealing fault or a flow boundary is shown in Figures 3.2. and 3.3. The plots are generated type-curve sets for the same value of dimensionless distance to the boundary and different values of the dimensionless group $C_D e^{2S}$.

The plots yield three regions: (1) the pure wellbore storage flow region, (2) the radial flow region and, (3) the "pseudo-steady state" flow region, due to the influence of the boundary. The last two flow regimes are similar to those developed for the case of no wellbore storage and no-skin effect, after the infinite-acting radial flow line is reached.

The following characteristics of the pressure and pressure derivative curves for a well near a no-flow boundary shown in Figure 3.2 may be considered:

(1) Unit slopes during early time for both pressure and pressure derivative which correspond to pure wellbore storage flow

(2) Maximum points of the derivative curves on the wellbore storage dominated flow region with the coordinates $\left[\left(\frac{t_D}{C_D}\right)P_D'\right]_x$ and $\left(\frac{t_D}{C_D}\right)_x$.

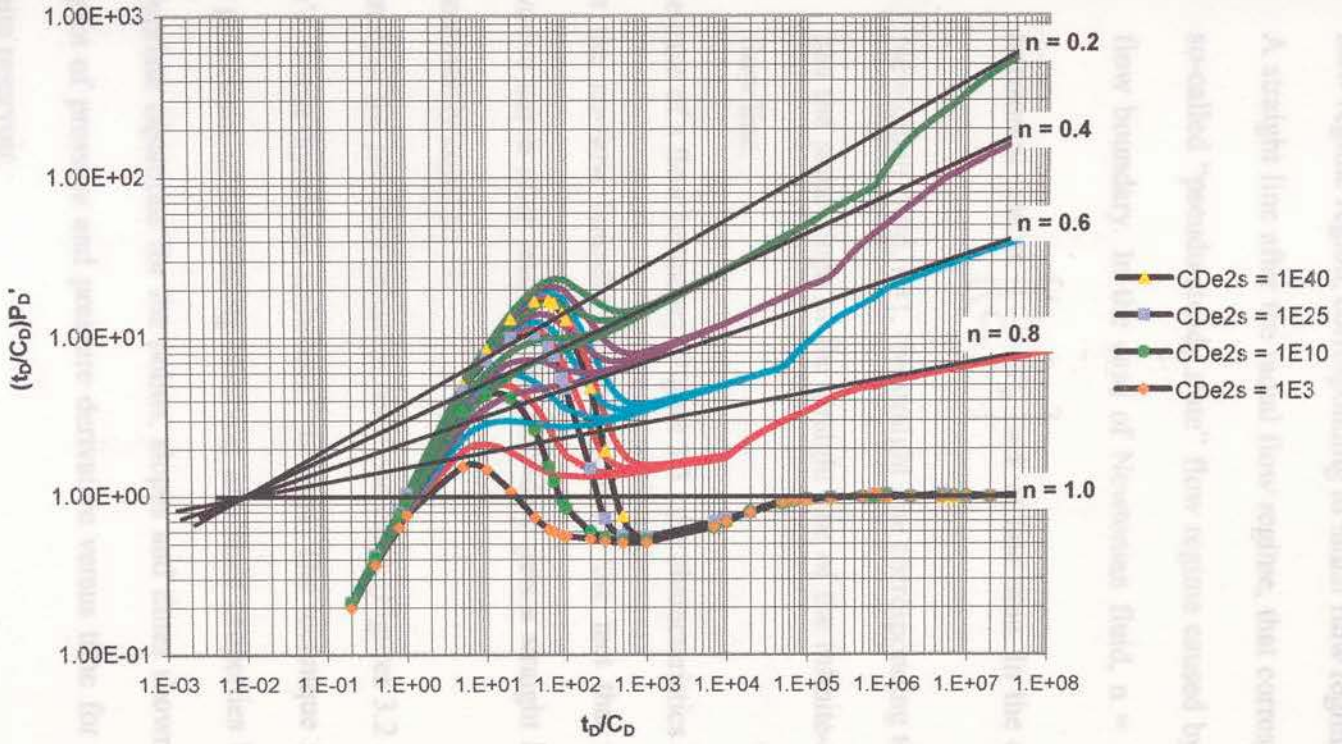

3.2 - Pressure derivative curves for a well near a no-flow boundary

(3) A straight line at late time, following the pure wellbore storage flow regime region, corresponding to radial flow regime.

(4) A straight line after the radial flow regime, that corresponds to the so-called "pseudo-steady state" flow regime caused by a linear no flow boundary. In the case of Newtonian fluid, n = 1, there is a horizontal line at $\left[\left(\frac{t_D}{C_D}\right)P_D'\right]=1$ at late time. In the case of non-Newtonian fluid, n≠1, the straight line corresponding to this region has the same slope as the straight line of the infinite-acting radial flow line.

In the case of a flow boundary, Figure 3.3., the characteristics are the same as in the no-flow boundary case except for the fact that the pressure derivative curve after reaching the boundary gets a straight line of slope approximately equal to –1.

To analyze the pressure behavior for those cases (Figures 3.2 and 3.3), the Tiab's Direct Synthesis technique[31] is used. The technique is a step-by-step procedure of calculating reservoir and fluid properties by using the appropriate equations for the points, slopes and times shown by the log-log plot of pressure and pressure derivative versus time for a well in an infinite reservoir.

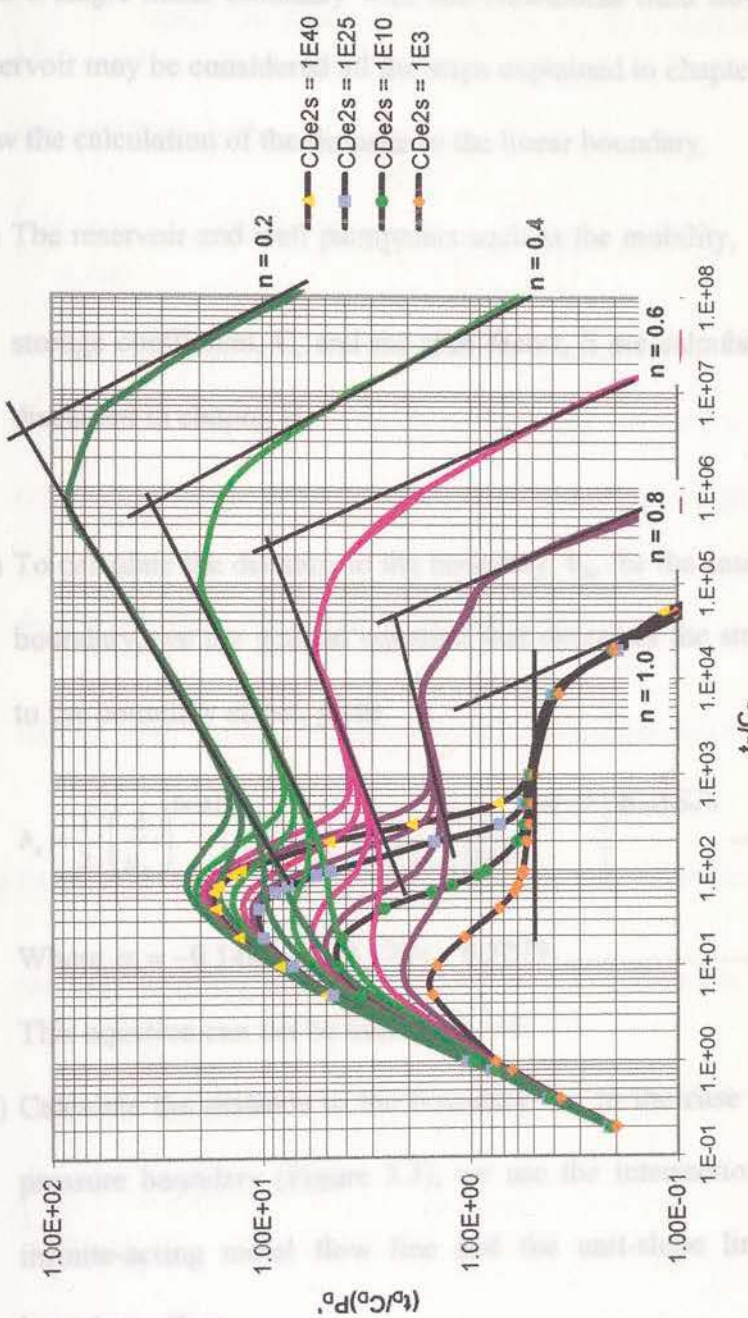

3.3.- Pressure derivative curves for a well near a constant-pressure boundary

The characteristics of the pressure and pressure derivative curves of a well near a single linear boundary with non-Newtonian fluid flow through the reservoir may be considered all the steps explained in chapter II, including now the calculation of the distance to the linear boundary.

(1) The reservoir and well parameters such as the mobility, $\frac{k}{\mu_e}$, wellbore storage coefficient, C, and the skin factor, S are calculated exactly as discussed in chapter II.

(2) To calculate the distance to the boundary, b_x, for the case of a no-flow boundary, we the general equation that describes the straight line due to the boundary effect, gives:

$$b_x = \frac{1}{2}\left[\left(\frac{k}{\mu_e}\right)^{(\alpha-1)}\left(\frac{t_{bx}q}{C}r_w^2\right)^{\alpha}\frac{1}{(t\Delta P')_{bx}}\left(\frac{q}{(2\pi h)}\right)^{n(1-\alpha)}\right]^{\frac{1}{n(1-\alpha)+3\alpha-1}} \quad \text{.....(3.6)}$$

Where $\alpha = -0.1486n^2 - 0.178n + 0.3279$ .....(3.7)

This equation can not be used for n = 1.

(3) Calculate the distance to the boundary, b_x, in the case of a constant-pressure boundary (Figure 3.3), we use the intersection point of the infinite-acting radial flow line and the unit-slope line due to the boundary effect.

Figure 3.4, which is a plot of the dimensionless time of the intersection $\left(\frac{t_D}{C_D}\right)_{irbx}$ versus the flow behavior index, n, for a well near a constant pressure boundary.

$$\left(\frac{t_D}{C_D}\right)_{irbx} = 1x10^{7} e^{-7.0143n} \quad \text{.....(3.8)}$$

Substituting Eqs. 2.4, 2.5 and 2.6 and evaluating for the time of the intersection and taking into the account that the radius of the well is represented by the distance to the linear boundary, we get:

$$b_x = \frac{1}{2}\left[\frac{1}{1x10^{7} e^{-7.0143n}} \frac{k}{\mu_e} \frac{(2\pi h)^n q^{1-n}}{C} r_w^2 t_{irbx}\right]^{\frac{1}{3-n}} \quad \text{.....(3.9)}$$

where "irbx" stands for intersection of radial flow and boundary lines.

(4) From Figure 3.5 which is a plot of the dimensionless time at the end of the infinite-acting radial flow line $\left(\frac{t_D}{C_D}\right)_{erf}$ versus the flow behavior index, n, for a well near a no-flow or a constant-pressure boundary.

$$\left(\frac{t_D}{C_D}\right)_{erf} = 3x10^{6} e^{-6.7962n} \quad \text{.....(3.10)}$$

Substituting Eqs. 2.4, 2.5 and 2.6, evaluating for the time and taking into the account that the radius of the well is represented by the distance to the linear boundary, we get:

$$b_x = \frac{1}{2}\left[\frac{1}{3x10^6 e^{6.7962n}}\frac{k}{\mu_e}\frac{(2\pi h)^n q^{1-n}}{C} r_w^2 t_{erf}\right]^{\frac{1}{3-n}} \quad \text{.....(3.11)}$$

Where "erf" stands for end of radial flow line.

Eq. 3.11 can be used in the case that the pressure derivative curve does not have noise and one can read the time at the end of the infinite-acting radial flow line or/and verification purposes.

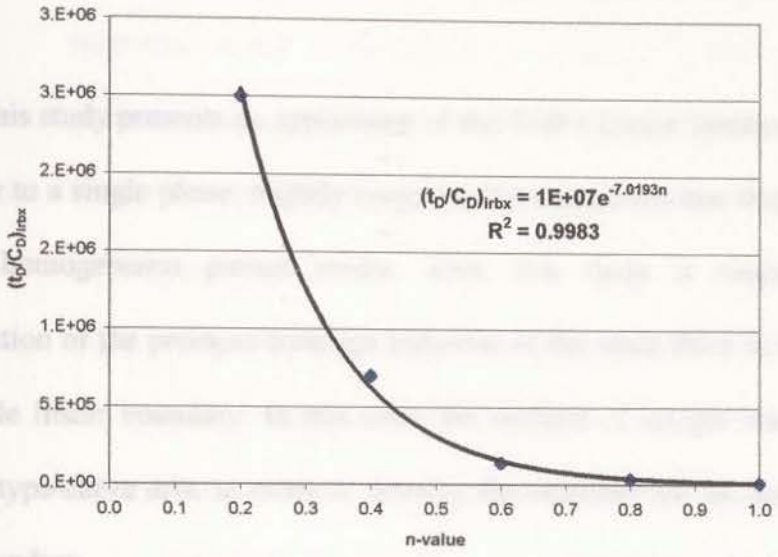

3.4 - Relationship between intersection of the radial flow and constant pressure lines and **n**

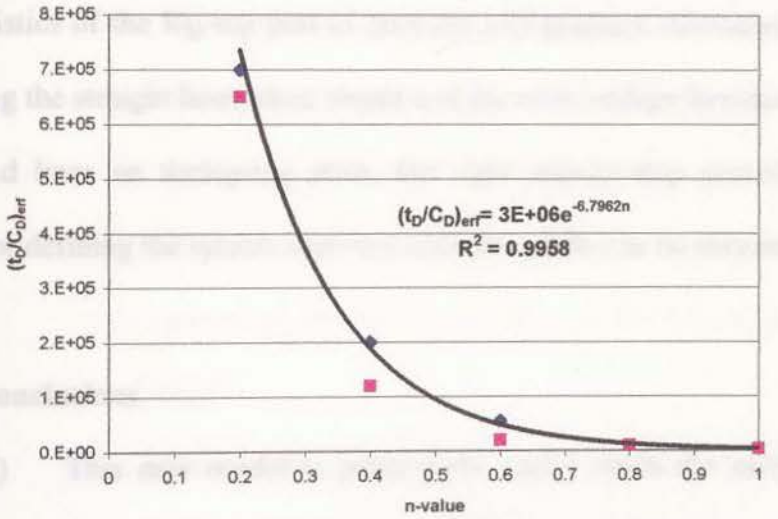

Figure 3.5 - Relationship between end of radial flow lines and flow behavior index in the presence of no-flow and/or constant pressure boundaries

CHAPTER IV

SUMMARY, CONCLUSIONS AND RECOMMENDATIONS

This study presents an application of the Tiab's Direct Synthesis[31] analysis technique to a single phase, slightly compressible and power-law fluid flow in an infinite, homogeneous porous media. Also, this study is extended to the interpretation of the pressure transient behavior of the same fluid in the presence of a single linear boundary. In this case, the method of images was utilized to generate type-curve sets, in order to develop the equation for the distance to the linear boundary.

The TDS technique developed in chapter II implies the recognition of unique characteristics of the log-log plot of pressure and pressure derivative curves. By identifying the straight lines, their slopes and the relationships between the unique points and lines on thelog-log plots, the right step-by-step procedure can be applied for defining the system and very reliable results can be obtained.

4.1) Conclusions

(1) This new model is particularly useful when the early-time unit-slope and/or the late-time infinite-acting radial flow lines are not observed or are not well defined due to the variety of reasons, such as lack of points, noise and interference of boundaries.

(2) Unlike type-curve Matching, the results obtained by this method are verifiable. Any parameter calculated is verified by a second equation, which corresponds to another feature relating the parameter.

(3) From the plots generated in this study we can conclude the following:

(a) The flow behavior index can be calculated from slope of the infinite-acting radial flow line

(b) The mobility value is calculated in many ways and definitely it is a function of the flow behavior index, n. First, we can use the intersection of the infinite-acting radial flow and the unit-slope lines. It is also given by the equation that describes the infinite-acting radial flow regime. It can be verified using the expression obtained from the infinite-acting radial flow line and the peaks generated for different values of the dimensionless group C_De^{2s}.

(c) The peaks generated for different values of C_De^{2s} give the skin factor.

(d) The distance to the nearest boundary can be calculated either using the end time of the infinite-acting radial flow

line or using the characteristic points observed in the plots such as the intersection time of the infinite-acting radial flow and the pseudo-steady flow lines in the case of constant-pressure boundary or the equation that describes the pseudo-state flow regime in the case of no-flow boundary.

(4) A Considerable number of approximations and models exists for analyzing well test data from different types of reservoirs and heterogeneities. Almost all the models assume Newtonian fluid flow even though the treatment fluids use in some operations such drilling, workover and enhanced oil-recovery processes are non-Newtonian. The resulting analysis would without doubt be erroneous because non-Newtonian fluids behave rather differently.

4.2) Recommendations

1. The Tiab's Direct Synthesis[31] technique can be extended to mixed boundary systems and to closed systems in the presence of non-Newtonian fluids.
2. Pressure transient analysis for horizontal wells has gained a lot of attention, especially for the production of heavy oil reservoirs. Due to the behavior of heavy oil as a non-Newtonian fluid, this work should be extended to this type of wells.

NOMENCLATURE

B	Formation volume factor, RB/STB
b_x	distance to the furthest boundary
b_{XD}	dimensionless distance to the image well on x-direction
c	compressibility, psi^{-1}
c_f	formation compressibility, psi^{-1}
c_t	total compressibility, psi^{-1}
C	wellbore storage coefficient, RB/psi
C_D	Dimensionless wellbore storage
C_De^{2S}	wellbore storage and skin dimensionless group
h	Formation thickness, ft
k	Permeability, mD
K_v	modified Bessel function of second kind of v order
n	Flow behavior index
P	Pressure, psi
P'	pressure derivative, psi/hour
P_D	Dimensionless pressure
P_{Dw}	dimensionless pressure at the wellbore
P_D'	Dimensionless pressure derivative
q	Flow rate, STB/D
r	radius of the flow, ft

r_w wellbore radius, ft

r_D dimensionless wellbore radius

r_{DI} dimesionless distance to the image well

r_{Dw} dimensionless distance to the real well

S Skin factor

t test time, hours

T temperature, °F

t_D dimensionless time

u Darcy's velocity, ft/sec

V Volume, ft^3

z Laplace variable

μ Viscosity, cp.

ϕ Porosity, faction

ρ Density of the fluid, lb_m/ft^3

α constant

β constant

δ constant

γ constant

Γ constant

Ψ constant

Subscripts:

eff	effective
erf	end of the radial flow line
i	intersection
irbx	intersection of radial flow and boundary lines
r	radial
SR	starting radial flow
x	maximum point

REFERENCES

[1] Muskat, M.: **"Use of Data on the Buildup of Bottom Hole Pressure"**, Trans. AIME (1937), 123,44

[2] Miller, C.C., Dyes, A.B., and Hutchinson, C.A., Jr.: **"The estimation of Permeability and Reservoir Pressure from Bottom Hole Pressure Buildup Characteristics"**, Trans. AIME (1950), 189,91

[3] Horner, D.R.: **"Pressure Buildup in Wells"**, Proceedings of the third world Petroleum Congress (II), (1951), The Hague, 503

[4] Ramey, H.J., Jr.: **" Short Time Well Test Data Interpretation in the Presence of Skin Effect and Wellbore Storage"**, Journal of Petroleum Technology, (Jan.1970), 97

[5] Tiab, D.: **"A New Approach to Detect and Locate Multiple Reservoir Boundaries by Transient well Pressure Data"**, MSThesis, New Mexico Institute of Mining and Technology, Socorro, New Mexico (1975)

[6] Tiab, D. and Kumar, A.: **"Application of P_D Function to Interference Analysis"**, paper SPE 6053

[7] Hughes, W.F.: **"An Introduction to Viscous Flow",** McGraw-Hill Book Company, 1979. pp 54-71

[8] Sadowski, T.J. and Bird, R.B.: **"Non-Newtonian flow through Porous Media, I. Theoretical"**, Trans. Soc. Rheol. (1965), vol.9, part.2, pp.243-250

[9] Sadowski, T.J.: **"Non-Newtonian Flow Through Porous Media, II. Experimental"**, Trans. Soc.Rheol. (1965), Vol.9, part. 2, pp.251-271

[10] Astarita, G. Letter. Cdn.J.Chem. Eng. Feb,1966. Pp.59-60

[11] Savins, J.G.: **Non-Newtonian Flow through Porous Media"**, Ind.and Eng. Chem. Fund., Oct.1969, pp.18-47

[12] Marshall, R.J. and Metzner, A.B.: **"Flow of Viscoelastic Fluid through Porous Media"**, Ind. And Eng. Chem. Fund. Aug. 1967. Pp.145-147

[13] Wissler, E.H.: **" Viscoelastic Effects in the Flow of Non-Newtonian Fluids through a Porous Medium"**, Ind. And Eng. Chem. Fund. 10, No.3(1971)mpp.411-417

[14] Schummer, Von P.: **"Zum Fliebverhalten Nicht-Newtonscher Flussigkeiten in Konischer Duesn"**, Rheol. ACTA, 7,No.3 (1968)

[15] Seyer, F.A. and Metzner, A.B.: **Turbulent Flow Properties of Viscoelastic Fluids"**, Can.J. Chem. Eng. June(1967) pp.121-126

[16] Van Poollen, H.K. and Jargon, J.R.: **Steady-state and Unsteady-state Flow of Non-Newtonian Fluids through Porous Media"**, Soc. Pet. Eng. J. (March, 1969) pp. 80-88

[17] Odeh, A.S. and Yang, H.T.: **"Flow of Non-Newtonian Power-law Fluids through Porous Media"**, Soc.Pet. Eng. J. (June,1979) pp.155-163

[18] Ikoku, C.U. and Ramey, H.J., Jr.: **"Transient Flow of Non-Newtonian Power Law Fluids in Porous Media"**, Soc. Pet. Eng. J. (June, 1979) pp.164-174

[19] Ikoku, C.U. and Ramey, H.J., Jr.: **"Pressure behavior during polymer flow in Petroleum Reservoirs"**, ASME trans. J. Of Energy Resources Tech. (June, 1982)

[20] Ikoku, C.U. and Ramey, H.J., Jr.: **"Wellbore Storage and Skin Effects during the Transient Flow of Non-Newtonian Power Law Fluids in Porous Media"**, Soc. Pet. Eng. J. (feb., 1980), pp.25-38

[21] Lund, O. and Ikoku, C.U.: **Pressure Transient Behavior of Non-Newtonian/Newtonian Fluid Composite Reservoirs"**, Soc. Pet. Eng. J. (April, 1981), pp.271-280

[22] Huh, C. And Snow, T.M.: **Well testing with a Non-Newtonian Fluid in the Reservoir"**, paper SPE 14453, 1985

[23] Vongvuthipornchai, S. And Raghavan, R.: **"Well test Analysis of Data dominated by Storage and Skin: Non-Newtonian Power-Law Fluids"**, SPEFE (Dec, 1987)

[24] Olarewaju, J.: **"A Reservoir Model of Non-Newtonian Fluid Flow"**, paper SPE 25301, June 1992

[25] Argawal, R.G., Al-Hussainy, R. And Ramey. H.J.,Jr.: **"An Investigation of Wellbore Storage and Skin Effect in Unsteady Liquid Flow: I. Analitycal Treatment"**, Soc. Pet. Eng. J. (Sept. 1970) pp. 279-290

[26] McKinley, R.M.: **"Wellbore Transmissibility from After-Flow-Dominated Pressure Builup Data"**, JPT (July, 1971) pp. 863

[27] Tiab, D.: **" Analysis of Multiple Sealing Faults Systems ad Closed Rectangular Reservoirs by Type Curve Matching"**, Ph.D. Dissertation, The University of Oklahoma, Norman, Oklahoma (1976)

[28] Tiab, D., Chrichlow, H.B.: **"Pressure Analysis of Multiple-Sealing Faults System and Bounded Reservoirs by Type Curve Matching"**, SPEJ (Dec. 1979) pp. 378-392

[29] Bourdet, D., Ayoub, J.A. and Pirard, Y.M.: **"Use of Pressure Derivative in well Test Interpretation"**, paper SPE 12777 presented at the 1984 California Regional Meeting of Soc. of Pet. Eng. Of AIME held in Long Beach, California, April 11-13, 1984.

[30] Bourdet, D., White, T.M., Douglas, A.A. and Pirard, Y.M.: **"A New Set of Type Curves Simplifies Well Test Analysis"**, World Oil (May 1983) pp. 95-106

[31] Tiab, D.: **"Analysis of Pressure and Pressure Derivative Without Type-Curve Matching: I-Skin and Wellbore Storage"**, Paper 25476

prepared for presentation at the production Operation Symposium held in Oklahoma City, Ok, USA. March 21-23, 1993.

[32] Stephest,H.: **"Algorithm 368, Numerical Inversion of Laplace Transforms"**, D-5 Communications of the ACM (Jan. 1970), 13, No. 47-49

[33] Vongvuthipornchai, S.: **"Well Test analysis for Non-Newtonian Fluid flow"**, PhD. Dissertation, 1985. University of Tulsa, Tulsa, Oklahoma, USA.

[34] Matthews, C.S., Brons, F., and Hazebroek, P.: **" A Method for Determination of Average pressure in a Bounded Reservoir",** trans. AIME 201 (1954) pp. 182-191

[35] Jones, P: **Reservoir Limit Test on Gas well"**, JPT (june 1962) pp.613-19

[36] Van Pollen, H.K.; **"Drawdown Curves Give Angle Between Intersecting Faults"** OGJ (December 1965) pp. 71-75

APPENDIX A
COMPUTER PROGRAM

Program for the calculation of the dimensionless pressure data

```
PROGRAM thesis
double precision sum1,term1,B,CC,T,PD,L,Z
INTEGER J
INTEGER K,JA
COMMON/thesis1/SKIN,CD
COMMON/thesis2/XNFLOW,BXD
OPEN(UNIT=6,FILE='Data.dat',STATUS='OLD')
OPEN(UNIT=10,FILE='Results.out',STATUS='OLD')
READ(6,*)
READ(6,*)SKIN
READ(6,*)
READ(6,*)CD
READ(6,*)
READ(6,*)XNFLOW
READ(6,*)
READ(6,*)BXD
READ(6,*)
READ(6,*)K
READ(6,*)
WRITE(10,111)
111 FORMAT(6X,'TD',10X,'PD')
                    DO 70 JA=1,K
                    READ(6,*)T
                    N=8
                    B=LOG(2.0)/T
                    SUM1=0.0
                    DO 30 J=1,N
                    Z=B*J
                    CALL VI(J,CC)
                    TERM1=CC*L(Z)
                    SUM1=SUM1+TERM1
30      CONTINUE
                    PD=B*SUM1
                    WRITE(10,100)TD,PD
100 FORMAT(3X,9E2,1X,F16.6)
70      CONTINUE
                    STOP
                    END
                    INTEGER FUNCTION FACT(NX)
```

```
                INTEGER NX
                IF(NX.EQ.0) THEN
                FACT=1
                ELSE
                FACT=1
                DO 10 I=1,NX
                FACT=FACT*I
10 CONTINUE
                ENDIF
                RETURN
                END

                SUBROUTINE VI(A,BB)
                DOUBLE PRECISION BB
                INTEGER A,K,H,KK,KK1,KK2,KK3,KK4,FACT
                N=8
                NN=N/2
                IF(A.LT.NN) THEN
                H=A
                ELSE
                H=N/2
                ENDIF
                SUM=0.0
                IM=((A+1)/2)
                DO 20 K=IM,H
                KK=2*K
                KK1=N/2-K
                KK2=K-1
                KK3=A-K
                KK4=2*K-A
                XNUM=(K**(N/2.0)*FACT(KK))

      DENOM=FACT(KK1)*FACT(K)*FACT(KK2)*FACT(KK3)*FACT(KK
4)
                TERM=XNUM/DENOM
                SUM=SUM+TERM
20 CONTINUE
                BB=((-1)**((N/2)+A))*SUM
                RETURN
                END
```

```
      FUNCTION L(S)
      DOUBLE PRECISION S,L
COMMON/THESIS1/SKIN,CD
COMMON/THESIS2/XNFLOW,BXD

YNA=(1.0-XNFLOW)/(3.0-XNFLOW)
YNB=2.0/(3.0-XNFLOW)
XXX1=YNB*SQRT(S)
XXX2=YNB*SQRT(S)*((2*BXD)**(1/YNB))
IF (XNFLOW.EQ.1) THEN
UP=BESSK0(XXX1)+SKIN*SQRT(S)*BESSK1(XXX1)
UP1=((BXD)**((1-XNFLOW)/2))*BESSK0(xxx2)
DOWN1=S*(SQRT(S)*BESSK1(XXX1)+
S*CD*(((BXD)**((1-XNFLOW)/2))*BESSK0(XXX2)
+SKIN*SQRT(S)*BESSK1(XXX1)))
DOWN1=S*(SQRT(S)*BESSK1(XXX1))
ELSE
UP=BESSKA(XXX1)+SKIN*SQRT(S)*BESSKB(XXX1)
UP1=((2*BXD)**((1-XNFLOW)/2))*BESSKA(XXX2)
DOWN=S*(SQRT(S)*BESSKB(XXX1)+
S*CD*(BESSKA(XXX1)+SKIN*SQRT(S)*BESSKB(XXX1)))
DOWN1=S*(SQRT(S)*BESSKB(XXX1)+
S*CD*(((2*BXD)**((1-XNFLOW)/2))*besska(XXX2)
+SKIN*SQRT(S)*BESSKB(XXX1)))
ENDIF
L=UP/DOWN+UP1/DOWN1
RETURN
END
REAL FUNCTION BESSKA(YXA)
REAL YXA
COMMON/THESIS2/XNFLOW
PI=3.141592654
YNA=(1.0-XNFLOW)/(3.0-XNFLOW)
BESSKA=(PI/(2.0*SIN(YNA*PI)))
*((YXA/2.0)**(-YNA)*(1.0/EXP(GAMMLN(1.0-YNA))
+(YXA**2.0/4.0)/EXP(GAMMLN(2.0-YNA)))-
(YXA/2.0)**(YNA)*(1.0/EXP(GAMMLN(1.0+YNA))
+(YXA**2.0/4.0)/EXP(GAMMLN(2.0+YNA))))
RETURN
END
```

```
      REAL FUNCTION BESSKB(YXB)
      REAL YXB
      COMMON/THESIS2/XNFLOW
      PI=3.141592654
      YNB=2.0/(3.0-XNFLOW)
      BESSKB=(PI/(2.0*SIN(YNB*PI)))
      *((YXB/2.0)**(-YNB)*(1.0/EXP(GAMMLN(1.0-YNB))
      +(YXB**2.0/4.0)/EXP(GAMMLN(2.0-YNB)))-
      (YXB/2.0)**(YNB)*(1.0/EXP(GAMMLN(1.0+YNB))
      +(YXB**2.0/4.0)/EXP(GAMMLN(2.0+YNB))))
      RETURN
      END

      REAL FUNCTION YI1(YX1,YN1)
      INTEGER FACT,I1
      SUMYI1=0.0
      DO 40 I1=1,1000
      YN1XX=YN1+I1+1.0
      DDD1=FACT(I1)*EXP(gammln(YN1XX))
      IF(DDD1.LE.0.0)GOTO 444
      TRMYI1=(YX1/2.0)**(YN1+2.0*I1)/(FACT(I1)
      *EXP(gammln(YN1XX)))
      SUMYI1=SUMYI1+TRMYI1
40    CONTINUE
444 YI1=SUMYI1
      RETURN
      END

      REAL FUNCTION YI2(YX2,YN2)
      INTEGER FACT,I2
      SUMYI2=0.0
      DO 40 I2=1,1000
      YN2XX=I2+1.0-YN2
      DDD2=FACT(I2)*EXP(gammln(YN2XX))
      IF(DDD2.LE.0.0)GOTO 445
      TRMYI2=(YX2/2.0)**(2.0*I2-YN2)/(FACT(I2)
      *EXP(gammln(YN2XX)))
      SUMYI2=SUMYI2+TRMYI2
40    CONTINUE
445 YI2=SUMYI2
      RETURN
```

```
      END
      FUNCTION gammln(xx)
      REAL gammln,xx
      INTEGER j
      DOUBLE PRECISION ser,stp,tmp,x,y,cof(6)
      SAVE cof,stp
      DATA cof,stp/76.18009172947146,-86.50532032941677,
     24.01409824083091,-.231739572450155,0.001208650973866179,
     -0.000005395239384953,2.5066282746310005/
      x=xx
      y=x
      tmp=x+5.5
      tmp=(x+0.5)*log(tmp)-tmp
      ser=1.000000000190015
      do 11 j=1,6
      y=y+1.0
      ser=ser+cof(j)/y
11    CONTINUE
      gammln=tmp+log(stp*ser/x)
      return
      END
!     (C) Copr. 1986-02 Numerical Recipes Softwate &j$$9R3#1">.


      FUNCTION bessk0(x)
      REAL bessk0,x
      REAL bessi0
      DOUBLE PRECISION p1,p2,p3,p4,p5,p6,p7,q1,q2,q3,
     q4,q5,q6,q7,y
      SAVE p1,p2,p3,p4,p5,p6,p7,q1,q2,q3,q4,q5,q6,q7
      DATA p1,p2,p3,p4,p5,p6,p7/-0.57721566,0.42278420,
     0.23069756,
     0.03488590,0.00262698,0.00010750,0.0000074/
      DATA q1,q2,q3,q4,q5,q6,q7/1.25331414,-0.07832358,
     0.02189568,-0.01062446,0.00587872,-0.00251540,0.00053208/
      if(x.le.2.0) then
      y=x*x/4.0
      bessk0=(-log(x/2.0)*bessi0(x))
     +(p1+y*(p2+y*(p3+y*(p4+y*(p5+y*(p6+y*p7))))))
      else
```

```
      y=(2.0/x)
      bessk0=(exp(-x)/sqrt(x))*
     (q1+y*(q2+y*(q3+y*(q4+y*(q5+y*(q6+y*q7))))))
      endif
      return
      END
!     (C)copr. 1986-92 Numerical Recipes Software &j$$9R3#1">.

      FUNCTION bessi0(x)
      REAL bessi0,x
      REAL ax
      DOUBLE PRECISION p1,p2,p3,p4,p5,p6,p7,q1,q2,q3,q4,q5,
     q6,q7,q8,q9,y
      SAVE p1,p2,p3,p4,p5,p6,p7,q1,q2,q3,q4,q5,q6,q7,q8,q9
      DATA p1,p2,p3,p4,p5,p6,p7/1.0,3.5156229,3.0899424,1.2067492,
     0.2659732,0.0360768,0.0045813/
      DATA
     q1,q2,q3,q4,q5,q6,q7,q8,q9/0.39894228,0.01328592,0.00225319,
     -0.00157565,0.00916281,-0.02057706,0.02635537,
     -0.01647633,0.00392377/
      if (abs(x).lt.3.75) then
      y=(x/3.75)**2
      bessi0=p1+y*(p2+y*(p3+y*(p4+y*(p5+y*(p6+y*p7)))))
      else
      ax=abs(x)
      y=3.75/ax
      bessi0=(exp(ax)/sqrt(ax))*
     (q1+y*(q2+y*(q3+y*(q4+y*(q5+y*(q6+y*(q7+y*(q8+y*q9))))))))
      endif
      return
      END
!     (C) Copr. 1986-92 Numerical Recipes Software &j$$9R3#1">.


      FUNCTION bessk1(x)
      REAL bessk1,x
            REAL bessi1
            DOUBLE PRECISION p1,p2,p3,p4,p5,p6,p7,q1,q2,q3,q4,
            q5,q6,q7,y
            SAVE p1,p2,p3,p4,p5,p6,p7,q1,q2,q3,q4,q5,q6,q7
            DATA p1,p2,p3,p4,p5,p6,p7/1.0,0.15443144,-0.67278579,
```

```
-0.18156897,-0.01919402,-0.00110404,-0.00004686/
DATA q1,q2,q3,q4,q5,q6,q7/1.25331414,0.23498619,
-0.03655620,0.01504268,-0.00780353,0.00325614,-
0.00068245/
if (x.le.2.0) then
y=x*x/4.0
bessk1=(log(x/2.0)*bessi1(x))
+(1.0/x)*(p1+y*(p2+y*(p3+y*(p4+y*(p5+y*(p6+y*p7))))))
else
y=2.0/x
bessk1=(exp(-x)/sqrt(x))
*(q1+y*(q2+y*(q3+y*(q4+y*(q5+y*(q6+y*q7))))))
endif
return
END
!       (C)     Copr. 1986-92 Numerical Recipes Software &j$$9R3#1">.

FUNCTION bessi1(x)
REAL bessi1,x
REAL ax
DOUBLE PRECISION p1,p2,p3,p4,p5,p6,p7,q1,q2,q3,q4,q5,
q6,q7,q8,q9,y
SAVE p1,p2,p3,p4,p5,p6,p7,q1,q2,q3,q4,q5,q6,q7,q8,q9
DATA p1,p2,p3,p4,p5,p6,p7/0.5,0.87890594,0.51498869,
0.15084934,0.02658733,0.00301532,0.00032411/
DATA q1,q2,q3,q4,q5,q6,q7,q8,q9/0.39894228,-0.03988024,
-0.00362018,0.00163801,-0.01031555,0.02282967,
-0.02895312,0.01787654,-0.00420059/
if (abs(x).lt.3.75) then
y=(x/3.75)**2
bessi1=x*(p1+y*(p2+y*(p3+y*(p4+y*(p5+y*(p6+y*p7))))))
else
ax=abs(x)
y=3.75/ax
bessi1=(exp(ax)/sqrt(ax))*
(q1+y*(q2+y*(q3+y*(q4+y*(q5+y*(q6+y*(q7+y*(q8+y*q9))))))))
if (x.lt.0.) bessi1=-bessi1
endif
return
END
!       (C)     Copr. 1986-92 Numerical Recipes Software &j$$9R3#1">.
```

HECKMAN
BINDERY, INC.
Bound-To-Please
AUG 00
N. MANCHESTER, INDIANA 46962

OU–828-B

DATE DUE

ALL LIBRARY MATERIALS MUST
BE RETURNED AFTER TWO WEEKS
USE IF NEEDED BY ANOTHER
PATRON

THE UNIVERSITY OF OKLAHOMA LIBRARY

This volume is the property of the University of Oklahoma, but the literary rights of the author are a separate property and must be respected. Passages must not be copied or closely paraphrased without the previous written consent of the author. If the reader obtains any assistance from this volume, he must give proper credit in his own work.

I grant the University of Oklahoma Libraries permission to make a copy of my thesis upon the request of individuals or libraries. This permission is granted with the understanding that a copy will be provided for research purposes only, and that requestors will be informed of these restrictions.

NAME [redacted]

DATE [redacted]

A library which borrows this thesis for use by its patrons is expected to secure the signature of each user.

This thesis by IRINA DESIREE KATIME MEINDL has been used by the following persons, whose signatures attest their acceptance of the above restrictions.

NAME AND ADDRESS	DATE